Search for chargino-neutralino production in *pp* collisions at s√=1.96 TeV with high-p_T leptons

Collaborators: Clark, Allan Geoffrey; Hamilton, Andrew; Lefevre, Régis; Sfyrla, Anna; Shreyber, Irina; Vallecorsa, Sofia; Wu, Xin

How to cite

CDF Collaboration. Search for chargino-neutralino production in *pp* collisions at s√=1.96 TeV with high-p_T leptons. In: Physical review. D. Particles, fields, gravitation, and cosmology, 2008, vol. 77, n° 05, p. 052002. doi: 10.1103/PhysRevD.77.052002

This publication URL: https://archive-ouverte.unige.ch/unige:38476
Publication DOI: 10.1103/PhysRevD.77.052002

PHYSICAL REVIEW D **77,** 052002 (2008)

Search for chargino-neutralino production in $p\bar{p}$ collisions at $\sqrt{s} = 1.96$ TeV with high-p_T leptons

T. Aaltonen,[23] J. Adelman,[13] T. Akimoto,[54] M. G. Albrow,[17] B. Álvarez González,[11] S. Amerio,[42] D. Amidei,[34]
A. Anastassov,[51] A. Annovi,[19] J. Antos,[14] M. Aoki,[24] G. Apollinari,[17] A. Apresyan,[47] T. Arisawa,[56] A. Artikov,[15]
W. Ashmanskas,[17] A. Attal,[3] A. Aurisano,[52] F. Azfar,[41] P. Azzi-Bacchetta,[42] P. Azzurri,[45] N. Bacchetta,[42] W. Badgett,[17]
A. Barbaro-Galtieri,[28] V. E. Barnes,[47] B. A. Barnett,[25] S. Baroiant,[7] V. Bartsch,[30] G. Bauer,[32] P.-H. Beauchemin,[33]
F. Bedeschi,[45] P. Bednar,[14] S. Behari,[25] G. Bellettini,[45] J. Bellinger,[58] A. Belloni,[22] D. Benjamin,[16] A. Beretvas,[17]
J. Beringer,[28] T. Berry,[29] A. Bhatti,[49] M. Binkley,[17] D. Bisello,[42] I. Bizjak,[30] R. E. Blair,[2] C. Blocker,[6] B. Blumenfeld,[25]
A. Bocci,[16] A. Bodek,[48] V. Boisvert,[48] G. Bolla,[47] A. Bolshov,[32] D. Bortoletto,[47] J. Boudreau,[46] A. Boveia,[10] B. Brau,[10]
A. Bridgeman,[24] L. Brigliadori,[5] C. Bromberg,[35] E. Brubaker,[13] J. Budagov,[15] H. S. Budd,[48] S. Budd,[24] K. Burkett,[17]
G. Busetto,[42] P. Bussey,[21] A. Buzatu,[33] K. L. Byrum,[2] S. Cabrera,[16,r] M. Campanelli,[35] M. Campbell,[34] F. Canelli,[17]
A. Canepa,[44] D. Carlsmith,[58] R. Carosi,[45] S. Carrillo,[18,l] S. Carron,[33] B. Casal,[11] M. Casarsa,[17] A. Castro,[5] P. Catastini,[45]
D. Cauz,[53] M. Cavalli-Sforza,[3] A. Cerri,[28] L. Cerrito,[30,p] S. H. Chang,[27] Y. C. Chen,[1] M. Chertok,[7] G. Chiarelli,[45]
G. Chlachidze,[17] F. Chlebana,[17] K. Cho,[27] D. Chokheli,[15] J. P. Chou,[22] G. Choudalakis,[32] S. H. Chuang,[51] K. Chung,[12]
W. H. Chung,[58] Y. S. Chung,[48] C. I. Ciobanu,[24] M. A. Ciocci,[45] A. Clark,[20] D. Clark,[6] G. Compostella,[42] M. E. Convery,[17]
J. Conway,[7] B. Cooper,[30] K. Copic,[34] M. Cordelli,[19] G. Cortiana,[42] F. Crescioli,[45] C. Cuenca Almenar,[7,r] J. Cuevas,[11,o]
R. Culbertson,[17] J. C. Cully,[34] D. Dagenhart,[17] M. Datta,[17] T. Davies,[21] P. de Barbaro,[48] S. De Cecco,[50] A. Deisher,[28]
G. De Lentdecker,[48,d] G. De Lorenzo,[3] M. Dell'Orso,[45] L. Demortier,[49] J. Deng,[16] M. Deninno,[5] D. De Pedis,[50]
P. F. Derwent,[17] G. P. Di Giovanni,[43] C. Dionisi,[50] B. Di Ruzza,[53] J. R. Dittmann,[4] M. D'Onofrio,[3] S. Donati,[45] P. Dong,[8]
J. Donini,[42] T. Dorigo,[42] S. Dube,[51] J. Efron,[38] R. Erbacher,[7] D. Errede,[24] S. Errede,[24] R. Eusebi,[17] H. C. Fang,[28]
S. Farrington,[29] W. T. Fedorko,[13] R. G. Feild,[59] M. Feindt,[26] J. P. Fernandez,[31] C. Ferrazza,[45] R. Field,[18] G. Flanagan,[47]
R. Forrest,[7] S. Forrester,[7] M. Franklin,[22] J. C. Freeman,[28] I. Furic,[18] M. Gallinaro,[49] J. Galyardt,[12] F. Garberson,[10]
J. E. Garcia,[45] A. F. Garfinkel,[47] K. Genser,[17] H. Gerberich,[24] D. Gerdes,[34] S. Giagu,[50] V. Giakoumopolou,[45,a]
P. Giannetti,[45] K. Gibson,[46] J. L. Gimmell,[48] C. M. Ginsburg,[17] N. Giokaris,[15,a] M. Giordani,[53] P. Giromini,[19] M. Giunta,[45]
V. Glagolev,[15] D. Glenzinski,[17] M. Gold,[36] N. Goldschmidt,[18] A. Golossanov,[17] G. Gomez,[11] G. Gomez-Ceballos,[32]
M. Goncharov,[52] O. González,[31] I. Gorelov,[36] A. T. Goshaw,[16] K. Goulianos,[49] A. Gresele,[42] S. Grinstein,[22]
C. Grosso-Pilcher,[13] R. C. Group,[17] U. Grundler,[24] J. Guimaraes da Costa,[22] Z. Gunay-Unalan,[35] C. Haber,[28] K. Hahn,[32]
S. R. Hahn,[17] E. Halkiadakis,[51] A. Hamilton,[20] B.-Y. Han,[48] J. Y. Han,[48] R. Handler,[58] F. Happacher,[19] K. Hara,[54]
D. Hare,[51] M. Hare,[55] S. Harper,[41] R. F. Harr,[57] R. M. Harris,[17] M. Hartz,[46] K. Hatakeyama,[49] J. Hauser,[8] C. Hays,[41]
M. Heck,[26] A. Heijboer,[44] B. Heinemann,[28] J. Heinrich,[44] C. Henderson,[32] M. Herndon,[58] J. Heuser,[26] S. Hewamanage,[4]
D. Hidas,[16] C. S. Hill,[10,c] D. Hirschbuehl,[26] A. Hocker,[17] S. Hou,[1] M. Houlden,[29] S.-C. Hsu,[9] B. T. Huffman,[41]
R. E. Hughes,[38] U. Husemann,[59] J. Huston,[35] J. Incandela,[10] G. Introzzi,[45] M. Iori,[50] A. Ivanov,[7] B. Iyutin,[32] E. James,[17]
B. Jayatilaka,[16] D. Jeans,[50] E. J. Jeon,[27] S. Jindariani,[18] W. Johnson,[7] M. Jones,[47] K. K. Joo,[27] S. Y. Jun,[12] J. E. Jung,[27]
T. R. Junk,[24] T. Kamon,[52] D. Kar,[18] P. E. Karchin,[57] Y. Kato,[40] R. Kephart,[17] U. Kerzel,[26] V. Khotilovich,[52] B. Kilminster,[38]
D. H. Kim,[27] H. S. Kim,[27] J. E. Kim,[27] M. J. Kim,[17] S. B. Kim,[27] S. H. Kim,[54] Y. K. Kim,[13] N. Kimura,[54] L. Kirsch,[6]
S. Klimenko,[18] M. Klute,[32] B. Knuteson,[32] B. R. Ko,[16] S. A. Koay,[10] K. Kondo,[56] D. J. Kong,[27] J. Konigsberg,[18]
A. Korytov,[18] A. V. Kotwal,[16] J. Kraus,[24] M. Kreps,[26] J. Kroll,[44] N. Krumnack,[4] M. Kruse,[16] V. Krutelyov,[10] T. Kubo,[54]
S. E. Kuhlmann,[2] T. Kuhr,[26] N. P. Kulkarni,[57] Y. Kusakabe,[56] S. Kwang,[13] A. T. Laasanen,[47] S. Lai,[33] S. Lami,[45]
S. Lammel,[17] M. Lancaster,[30] R. L. Lander,[7] K. Lannon,[38] A. Lath,[51] G. Latino,[45] I. Lazzizzera,[42] T. LeCompte,[2] J. Lee,[48]
J. Lee,[27] Y. J. Lee,[27] S. W. Lee,[52,q] R. Lefèvre,[20] N. Leonardo,[32] S. Leone,[45] S. Levy,[13] J. D. Lewis,[17] C. Lin,[59] C. S. Lin,[28]
J. Linacre,[41] M. Lindgren,[17] E. Lipeles,[9] A. Lister,[7] D. O. Litvintsev,[17] T. Liu,[17] N. S. Lockyer,[44] A. Loginov,[59] M. Loreti,[42]
L. Lovas,[14] R.-S. Lu,[1] D. Lucchesi,[42] J. Lueck,[26] C. Luci,[50] P. Lujan,[28] P. Lukens,[17] G. Lungu,[18] L. Lyons,[41] J. Lys,[28]
R. Lysak,[14] E. Lytken,[47] P. Mack,[26] D. MacQueen,[33] R. Madrak,[17] K. Maeshima,[17] K. Makhoul,[32] T. Maki,[23]
P. Maksimovic,[25] S. Malde,[41] S. Malik,[30] G. Manca,[29] A. Manousakis,[15,a] F. Margaroli,[47] C. Marino,[26] C. P. Marino,[24]
A. Martin,[59] M. Martin,[25] V. Martin,[21,j] M. Martínez,[3] R. Martínez-Ballarín,[31] T. Maruyama,[54] P. Mastrandrea,[50]
T. Masubuchi,[54] M. E. Mattson,[57] P. Mazzanti,[5] K. S. McFarland,[48] P. McIntyre,[52] R. McNulty,[29,i] A. Mehta,[29]
P. Mehtala,[23] S. Menzemer,[11,k] A. Menzione,[45] P. Merkel,[47] C. Mesropian,[49] A. Messina,[35] T. Miao,[17] N. Miladinovic,[6]
J. Miles,[32] R. Miller,[35] C. Mills,[22] M. Milnik,[26] A. Mitra,[1] G. Mitselmakher,[18] H. Miyake,[54] S. Moed,[22] N. Moggi,[5]
C. S. Moon,[27] R. Moore,[17] M. Morello,[45] P. Movilla Fernandez,[28] J. Mülmenstädt,[28] A. Mukherjee,[17] Th. Muller,[26]
R. Mumford,[25] P. Murat,[17] M. Mussini,[5] J. Nachtman,[17] Y. Nagai,[54] A. Nagano,[54] J. Naganoma,[56] K. Nakamura,[54]

1550-7998/2008/77(5)/052002(20)

I. Nakano,[39] A. Napier,[55] V. Necula,[16] C. Neu,[44] M. S. Neubauer,[24] J. Nielsen,[28,f] L. Nodulman,[2] M. Norman,[9] O. Norniella,[24] E. Nurse,[30] S. H. Oh,[16] Y. D. Oh,[27] I. Oksuzian,[18] T. Okusawa,[40] R. Oldeman,[29] R. Orava,[23] K. Osterberg,[23] S. Pagan Griso,[42] C. Pagliarone,[45] E. Palencia,[17] V. Papadimitriou,[17] A. Papaikonomou,[26] A. A. Paramonov,[13] B. Parks,[38] S. Pashapour,[33] J. Patrick,[17] G. Pauletta,[53] M. Paulini,[12] C. Paus,[32] D. E. Pellett,[7] A. Penzo,[53] T. J. Phillips,[16] G. Piacentino,[45] J. Piedra,[43] L. Pinera,[18] K. Pitts,[24] C. Plager,[8] L. Pondrom,[58] X. Portell,[3] O. Poukhov,[15] N. Pounder,[41] F. Prakoshyn,[15] A. Pronko,[17] J. Proudfoot,[2] F. Ptohos,[17,h] G. Punzi,[45] J. Pursley,[58] J. Rademacker,[41,c] A. Rahaman,[46] V. Ramakrishnan,[58] N. Ranjan,[47] I. Redondo,[31] B. Reisert,[17] V. Rekovic,[36] P. Renton,[41] M. Rescigno,[50] S. Richter,[26] F. Rimondi,[5] L. Ristori,[45] A. Robson,[21] T. Rodrigo,[11] E. Rogers,[24] S. Rolli,[55] R. Roser,[17] M. Rossi,[53] R. Rossin,[10] P. Roy,[33] A. Ruiz,[11] J. Russ,[12] V. Rusu,[17] H. Saarikko,[23] A. Safonov,[52] W. K. Sakumoto,[48] G. Salamanna,[50] O. Saltó,[3] L. Santi,[53] S. Sarkar,[50] L. Sartori,[45] K. Sato,[17] A. Savoy-Navarro,[43] T. Scheidle,[26] P. Schlabach,[17] E. E. Schmidt,[17] M. A. Schmidt,[13] M. P. Schmidt,[59] M. Schmitt,[37] T. Schwarz,[7] L. Scodellaro,[11] A. L. Scott,[10] A. Scribano,[45] F. Scuri,[45] A. Sedov,[47] S. Seidel,[36] Y. Seiya,[40] A. Semenov,[15] L. Sexton-Kennedy,[17] A. Sfyria,[20] S. Z. Shalhout,[57] M. D. Shapiro,[28] T. Shears,[29] P. F. Shepard,[46] D. Sherman,[22] M. Shimojima,[54,n] M. Shochet,[13] Y. Shon,[58] I. Shreyber,[20] A. Sidoti,[45] P. Sinervo,[33] A. Sisakyan,[15] A. J. Slaughter,[17] J. Slaunwhite,[38] K. Sliwa,[55] J. R. Smith,[7] F. D. Snider,[17] R. Snihur,[33] M. Soderberg,[34] A. Soha,[7] S. Somalwar,[51] V. Sorin,[35] J. Spalding,[17] F. Spinella,[45] T. Spreitzer,[33] P. Squillacioti,[45] M. Stanitzki,[59] R. St. Denis,[21] B. Stelzer,[8] O. Stelzer-Chilton,[41] D. Stentz,[37] J. Strologas,[36] D. Stuart,[10] J. S. Suh,[27] A. Sukhanov,[18] H. Sun,[55] I. Suslov,[15] T. Suzuki,[54] A. Taffard,[24,e] R. Takashima,[39] Y. Takeuchi,[54] R. Tanaka,[39] M. Tecchio,[34] P. K. Teng,[1] K. Terashi,[49] J. Thom,[17,g] A. S. Thompson,[21] G. A. Thompson,[24] E. Thomson,[44] P. Tipton,[59] V. Tiwari,[12] S. Tkaczyk,[17] D. Toback,[52] S. Tokar,[14] K. Tollefson,[35] T. Tomura,[54] D. Tonelli,[17] S. Torre,[19] D. Torretta,[17] S. Tourneur,[43] W. Trischuk,[33] Y. Tu,[44] N. Turini,[45] F. Ukegawa,[54] S. Uozumi,[54] S. Vallecorsa,[20] N. van Remortel,[23] A. Varganov,[34] E. Vataga,[36] F. Vázquez,[18,l] G. Velev,[17] C. Vellidis,[45,a] V. Veszpremi,[47] M. Vidal,[31] R. Vidal,[17] I. Vila,[11] R. Vilar,[11] T. Vine,[30] M. Vogel,[36] I. Volobouev,[28,q] G. Volpi,[45] F. Würthwein,[9] P. Wagner,[44] R. G. Wagner,[2] R. L. Wagner,[17] J. Wagner-Kuhr,[26] W. Wagner,[26] T. Wakisaka,[40] R. Wallny,[8] S. M. Wang,[1] A. Warburton,[33] D. Waters,[30] M. Weinberger,[52] W. C. Wester III,[17] B. Whitehouse,[55] D. Whiteson,[44,e] A. B. Wicklund,[2] E. Wicklund,[17] G. Williams,[33] H. H. Williams,[44] P. Wilson,[17] B. L. Winer,[38] P. Wittich,[17,g] S. Wolbers,[17] C. Wolfe,[13] T. Wright,[34] X. Wu,[20] S. M. Wynne,[29] A. Yagil,[9] K. Yamamoto,[40] J. Yamaoka,[51] T. Yamashita,[39] C. Yang,[59] U. K. Yang,[13,m] Y. C. Yang,[27] W. M. Yao,[28] G. P. Yeh,[17] J. Yoh,[17] K. Yorita,[13] T. Yoshida,[40] G. B. Yu,[48] I. Yu,[27] S. S. Yu,[17] J. C. Yun,[17] L. Zanello,[50] A. Zanetti,[53] I. Zaw,[22] X. Zhang,[24] Y. Zheng,[8,b] and S. Zucchelli[5]

(CDF Collaboration)

[1]*Institute of Physics, Academia Sinica, Taipei, Taiwan 11529, Republic of China*
[2]*Argonne National Laboratory, Argonne, Illinois 60439, USA*
[3]*Institut de Fisica d'Altes Energies, Universitat Autonoma de Barcelona, E-08193, Bellaterra (Barcelona), Spain*
[4]*Baylor University, Waco, Texas 76798, USA*
[5]*Istituto Nazionale di Fisica Nucleare, University of Bologna, I-40127 Bologna, Italy*
[6]*Brandeis University, Waltham, Massachusetts 02254, USA*
[7]*University of California, Davis, Davis, California 95616, USA*
[8]*University of California, Los Angeles, Los Angeles, California 90024, USA*
[9]*University of California, San Diego, La Jolla, California 92093, USA*
[10]*University of California, Santa Barbara, Santa Barbara, California 93106, USA*
[11]*Instituto de Fisica de Cantabria, CSIC-University of Cantabria, 39005 Santander, Spain*
[12]*Carnegie Mellon University, Pittsburgh, Pennsylvania 15213, USA*
[13]*Enrico Fermi Institute, University of Chicago, Chicago, Illinois 60637, USA*
[14]*Comenius University, 842 48 Bratislava, Slovakia and Institute of Experimental Physics, 040 01 Kosice, Slovakia*
[15]*Joint Institute for Nuclear Research, RU-141980 Dubna, Russia*
[16]*Duke University, Durham, North Carolina 27708, USA*
[17]*Fermi National Accelerator Laboratory, Batavia, Illinois 60510, USA*
[18]*University of Florida, Gainesville, Florida 32611, USA*
[19]*Laboratori Nazionali di Frascati, Istituto Nazionale di Fisica Nucleare, I-00044 Frascati, Italy*
[20]*University of Geneva, CH-1211 Geneva 4, Switzerland*
[21]*Glasgow University, Glasgow G12 8QQ, United Kingdom*
[22]*Harvard University, Cambridge, Massachusetts 02138, USA*
[23]*Division of High Energy Physics, Department of Physics, University of Helsinki*
and Helsinki Institute of Physics, FIN-00014, Helsinki, Finland

[24]*University of Illinois, Urbana, Illinois 61801, USA*
[25]*The Johns Hopkins University, Baltimore, Maryland 21218, USA*
[26]*Institut für Experimentelle Kernphysik, Universität Karlsruhe, 76128 Karlsruhe, Germany*
[27]*Center for High Energy Physics: Kyungpook National University, Daegu 702-701, Korea;*
Seoul National University, Seoul 151-742, Korea; Sungkyunkwan University, Suwon 440-746, Korea;
Korea Institute of Science and Technology Information, Daejeon, 305-806, Korea;
Chonnam National University, Gwangju, 500-757, Korea
[28]*Ernest Orlando Lawrence Berkeley National Laboratory, Berkeley, California 94720, USA*
[29]*University of Liverpool, Liverpool L69 7ZE, United Kingdom*
[30]*University College London, London WC1E 6BT, United Kingdom*
[31]*Centro de Investigaciones Energeticas Medioambientales y Tecnologicas, E-28040 Madrid, Spain*
[32]*Massachusetts Institute of Technology, Cambridge, Massachusetts 02139, USA*
[33]*Institute of Particle Physics: McGill University, Montréal, Canada H3A 2T8;*
and University of Toronto, Toronto, Canada M5S 1A7
[34]*University of Michigan, Ann Arbor, Michigan 48109, USA*
[35]*Michigan State University, East Lansing, Michigan 48824, USA*
[36]*University of New Mexico, Albuquerque, New Mexico 87131, USA*
[37]*Northwestern University, Evanston, Illinois 60208, USA*
[38]*The Ohio State University, Columbus, Ohio 43210, USA*
[39]*Okayama University, Okayama 700-8530, Japan*
[40]*Osaka City University, Osaka 588, Japan*
[41]*University of Oxford, Oxford OX1 3RH, United Kingdom*
[42]*University of Padova, Istituto Nazionale di Fisica Nucleare, Sezione di Padova-Trento, I-35131 Padova, Italy*
[43]*LPNHE, Universite Pierre et Marie Curie/IN2P3-CNRS, UMR7585, Paris, F-75252 France*
[44]*University of Pennsylvania, Philadelphia, Pennsylvania 19104, USA*
[45]*Istituto Nazionale di Fisica Nucleare Pisa, Universities of Pisa, Siena and Scuola Normale Superiore, I-56127 Pisa, Italy*
[46]*University of Pittsburgh, Pittsburgh, Pennsylvania 15260, USA*
[47]*Purdue University, West Lafayette, Indiana 47907, USA*
[48]*University of Rochester, Rochester, New York 14627, USA*
[49]*The Rockefeller University, New York, New York 10021, USA*
[50]*Istituto Nazionale di Fisica Nucleare, Sezione di Roma 1, University of Rome "La Sapienza," I-00185 Roma, Italy*
[51]*Rutgers University, Piscataway, New Jersey 08855, USA*
[52]*Texas A&M University, College Station, Texas 77843, USA*
[53]*Istituto Nazionale di Fisica Nucleare, University of Trieste/ Udine, Italy*
[54]*University of Tsukuba, Tsukuba, Ibaraki 305, Japan*
[55]*Tufts University, Medford, Massachusetts 02155, USA*
[56]*Waseda University, Tokyo 169, Japan*
[57]*Wayne State University, Detroit, Michigan 48201, USA*
[58]*University of Wisconsin, Madison, Wisconsin 53706, USA*
[59]*Yale University, New Haven, Connecticut 06520, USA*
(Received 22 November 2007; published 7 March 2008)

We present a search for the associated production of charginos and neutralinos in $p\bar{p}$ collisions at $\sqrt{s} = 1.96$ TeV. The data were collected at the Collider Detector at Fermilab (CDF II) and correspond to integrated luminosities between 0.7 and 1.0 fb^{-1}. We look for final states with one high-p_T electron or

---

[a] Visitor from University of Athens, 15784 Athens, Greece.

[b] Visitor from Chinese Academy of Sciences, Beijing 100864, China.

[c] Visitor from University of Bristol, Bristol BS8 1TL, United Kingdom.

[d] Visitor from University Libre de Bruxelles, B-1050 Brussels, Belgium.

[e] Visitor from University of California Irvine, Irvine, CA 92697, USA.

[f] Visitor from University of California Santa Cruz, Santa Cruz, CA 95064, USA.

[g] Visitor from Cornell University, Ithaca, NY 14853, USA.

[h] Visitor from University of Cyprus, Nicosia CY-1678, Cyprus.

[i] Visitor from University College Dublin, Dublin 4, Ireland.

[j] Visitor from University of Edinburgh, Edinburgh EH9 3JZ, United Kingdom.

[k] Visitor from University of Heidelberg, D-69120 Heidelberg, Germany.

[l] Visitor from Universidad Iberoamericana, Mexico D.F., Mexico.

[m] Visitor from University of Manchester, Manchester M13 9PL, United Kingdom.

[n] Visitor from Nagasaki Institute of Applied Science, Nagasaki, Japan.

[o] Visitor from University de Oviedo, E-33007 Oviedo, Spain.

[p] Visitor from Queen Mary, University of London, London, E1 4NS, United Kingdom.

[q] Visitor from Texas Tech University, Lubbock, TX 79409, USA.

[r] Visitor from IFIC (CSIC-Universitat de Valencia), 46071 Valencia, Spain.

muon, and two additional leptons. Our results are consistent with the standard model expectations, and we set limits on the cross section as a function of the chargino mass in three different supersymmetric scenarios. For a specific minimal supersymmetric standard model scenario with no slepton mixing, we set a 95% C.L. limit at 151 GeV/c^2.

DOI: 10.1103/PhysRevD.77.052002 PACS numbers: 14.80.Ly, 12.60.Jv, 13.85.Rm

I. INTRODUCTION

Supersymmetry [1,2] (SUSY) is a proposed symmetry of nature. It predicts the existence of supersymmetric partners for the standard model (SM) particles, called gauginos (Higgsinos) for the gauge (Higgs) bosons, and squarks/sleptons for fermions. The lightest SUSY particle is referred to as the LSP. If SUSY is an exact symmetry, the supersymmetric and the SM particles have the same mass, related couplings, and spin differing by 1/2. As a consequence of the nonobservation of light SUSY particles, such as the selectron, SUSY must be a broken symmetry, if realized. Several symmetry breaking models have been discussed in the past years. The gravitational interactions are responsible for the symmetry breaking in the minimal supergravity (mSUGRA) [3] scenario, whereas the ordinary gauge interactions are the source of SUSY breaking in the gauge-mediated supersymmetry breaking (GMSB) [2] model. In broken SUSY, gauginos and Higgsinos combine to form mass eigenstates called charginos ($\tilde{\chi}^{\pm}_{1,2}$) and neutralinos ($\tilde{\chi}^{0}_{1,2,3,4}$). The lightest neutralino, $\tilde{\chi}^0_1$, can be the LSP. SUSY is one of the most promising theories of physics beyond the SM as it can accommodate gravity and unify the gauge interactions. In SUSY models where R parity [4] is conserved, the LSP is stable and only weakly interacting, and thus is a viable dark matter candidate.

Experimental bounds on the gaugino masses are set by the LEP experiments at 103.5 GeV/c^2 for the lightest chargino, in scenarios with large sfermion masses [5], and at 50.3 GeV/c^2 for the lightest neutralino in mSUGRA. These constraints are very robust within mSUGRA-inspired SUSY models and do not depend on the chargino decay modes, except for a few pathological cases [6]. The D0 Collaboration excludes the chargino mass below 117 GeV/c^2 in a specific SUSY breaking scenario described in [7], where the standard mixing between the left and the right components in the third generation families is suppressed.

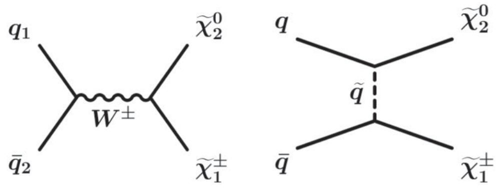

FIG. 1. Leading-order Feynman diagrams for chargino and neutralino associated production. The interaction is mediated through virtual W (left diagram) and squark ($\tilde{q}$, right diagram).

In this article we present a search for the associated production of the lightest chargino $\tilde{\chi}^{\pm}_1$ and the second-lightest neutralino $\tilde{\chi}^0_2$ (shown in Fig. 1), performed as a counting experiment in data collected by the CDF detector.

Charginos and neutralinos can be among the lightest SUSY particles in the models we explore, with associated production cross sections within the reach of the Tevatron collider [8]. If these sparticles decay leptonically within the detector, the final state is characterized by the presence of leptons and significant missing energy [9], $\not{E}_T$, due to particles escaping detection. While the process $\tilde{\chi}^{\pm}_1\tilde{\chi}^0_1 \to \ell\nu\tilde{\chi}^0_1\tilde{\chi}^0_1$ results in a final state with $\ell + \not{E}_T$, which has a large inclusive W background, the distinct signature of $\tilde{\chi}^{\pm}_1\tilde{\chi}^0_2 \to \ell\ell\ell\nu\tilde{\chi}^0_1$ makes the search for the associated production of the chargino $\tilde{\chi}^{\pm}_1$ and neutralino $\tilde{\chi}^0_2$ (see Fig. 2) one of the most powerful tests of SUSY at hadron colliders.

The paper is organized as follows. Section II contains a brief description of the CDF detector. Section III presents the lepton identification procedure and measurement of the misidentification rate. In Sec. IV we discuss the backgrounds, and in Sec. V we describe the event selection. In Sec. VI we present the estimated systematic uncertainties, followed by the validation of the analysis procedure in Sec. VII. The searches presented in this paper are not targeted at a specific model, but rather are designed to cover a large range of possible new physics scenarios in which events with three leptons and significant missing transverse energy are predicted at rates larger than the SM predictions. Nevertheless, based on the results presented in Sec. VIII, we set limits as a function of the chargino mass in several SUSY scenarios (Sec. IX). The results of the analysis presented in this paper are combined with results of similar searches carried out at CDF to further improve the sensitivity [10].

II. EXPERIMENTAL APPARATUS

The CDF II detector [11] is a general-purpose detector with approximate azimuthal and forward-backward symmetry. CDF combines precision charged-particle tracking with projective calorimeter towers and muon detection. In the detector coordinate system, ϕ is the azimuthal angle around the beam axis and η is the pseudorapidity defined as $\eta = -\ln\tan(\theta/2)$, where θ is the polar angle from the beam axis. The radial distance to the beam axis is referred to as r.

The tracking system is composed of an inner silicon detector ($1.5 < r < 29.0$ cm) and an outer drift chamber (COT, $40 < r < 140$ cm). These detectors provide three-

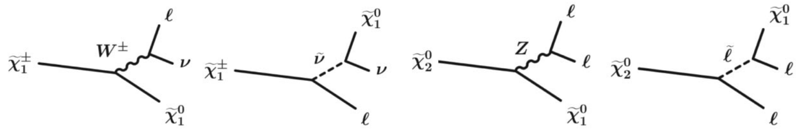

FIG. 2. Chargino and neutralino decay modes. The $\tilde{\ell}$ and the $\tilde{\nu}$ are the SUSY counterparts of the lepton and the neutrino.

dimensional vertex measurement and track reconstruction efficiency above 90% in the pseudorapidity range $|\eta| < 2.0$. For the leptons in our search, the resolution on the impact parameter is ≈ 40 μm, including ≈ 30 μm for the beam size. Surrounding the tracking system is a solenoidal magnet which provides a 1.4 T field aligned parallel to the beam. From the curvature of a track in the magnetic field, we determine the transverse momentum $p_{\rm T}$ of charged particles. The momentum resolution of the outer tracking is $\sigma(p_{\rm T})/p_{\rm T}^2 = 0.0017$ c/GeV.

Two layers of sampling calorimeters, one for detecting electromagnetic particles and the other to measure the remaining hadronic energy, cover the range $|\eta| < 3.6$. The central electromagnetic calorimeter (CEM) surrounds the solenoid within $|\eta| < 1.1$. It consists of lead sheets separated by polystyrene scintillator with an energy resolution of $13.5\%/\sqrt{E_{\rm T}} \oplus 1.5\%$, where $E_{\rm T} = |E| \sin\theta$ is measured in GeV. The CEM is segmented into 24 wedges per side; each wedge spans an angle of approximately 15 degrees in ϕ and is divided into ten towers of $\Delta\eta = 0.11$. At normal incidence the total depth corresponds to about 18 radiation lengths (X_0). A proportional chamber (CES) is embedded in each CEM wedge at the shower maximum and provides good spatial resolution and shower shape information used for electron and photon identification. The central hadronic calorimeter (CHA), positioned outside the CEM, matches the CEM segmentation into 24 wedges but uses steel absorbers interspersed with acrylic scintillators. There are 23 layers in the CHA and each layer is composed of one inch of steel and one centimeter of scintillator. The end wall calorimeter and the end plug calorimeter complete the coverage in the regions $0.8 < |\eta| < 1.2$ and $1.1 < |\eta| < 3.6$, respectively. The plug calorimeter consists of a lead-scintillator electromagnetic section (PEM) and an iron-scintillator hadronic section (PHA). The PEM resolution is $16\%/\sqrt{E_{\rm T}} \oplus 1\%$. The PEM also contains a shower maximum detector (PES).

The muon system is installed outside the calorimeters. The innermost four-layer drift chamber system (CMU) can detect minimum ionizing particles with transverse momenta larger than 1.4 GeV$/c$. An additional four-layer drift chamber (CMP) is located outside the magnet return yoke and detects particles with $p_{\rm T} > 2.0$ GeV$/c$. The CMU-CMP coverage ($|\eta| < 0.6$) is extended up to $|\eta| < 1.0$ by the central muon extension chambers (CMX). Outside the CMP and CMX chambers are scintillator detectors providing additional timing measurements. The last set of muon detectors (IMU) covers the region $1.0 < |\eta| < 1.5$. The information from the IMU chambers is not used in this analysis.

The luminosity is measured from the total inelastic $p\bar{p}$ cross section using Cherenkov counters located in the $3.7 < |\eta| < 4.7$ region.

The CDF trigger has a three-level architecture. The first level (L1) is a custom-designed hardware trigger which makes a fast trigger decision based on preliminary information from the tracking, calorimeter, and muon systems with an average accept rate of 25 kHz. The second level (L2) uses both custom hardware and a software-based event reconstruction with an accept rate of 750 Hz. The third level (L3) uses the offline reconstruction software and selects events for storage with a rate of up to 85 Hz [12].

III. LEPTON IDENTIFICATION

A. Lepton identification probability

We use different constraints on identification variables for high-$p_{\rm T}$ ($p_{\rm T} > 20$ GeV$/c$) and low-$p_{\rm T}$ ($p_{\rm T} < 20$ GeV$/c$) leptons due to different detection characteristics and also due to the trigger requirements. These identification criteria are described below and are summarized in Tables I, II, and III.

Reconstructed central tracks must have at least five hits out of 12 possible in at least three (two) out of four axial (stereo) COT super layers, to ensure high reconstruction efficiency and purity. We accept only tracks originating within ± 60 cm from the center of the detector, and we apply a cut on the impact parameter (d_0, see Table I) to suppress cosmic rays and secondary vertices. The impact parameter is the radial distance of closest approach between the track and the beam line. For each beam-constrained COT track, we place a requirement on the fit

TABLE I. Requirements for central tracks.

Variable	Cut
Number of axial COT super layers	≥ 3 with ≥ 5 hits
Number of stereo COT super layers	≥ 2 with ≥ 5 hits
$\lvert z_0\rvert$	<60 cm
$\lvert d_0\rvert$ (no silicon hits)	<0.2 cm
$\lvert d_0\rvert$ (silicon hits)	<0.02 cm
Muon tracks:	
COT exit radius (CMX)	>140 cm
χ^2 (first 350 pb^{-1})	<2.8
χ^2 (otherwise)	<2.3

TABLE II. Electron selection criteria.

Variable	Cut
Loose electron:	
Central track	
Not conversion	
$\vert\eta\vert$	<1
$E_{\mathrm{Had}}/E_{\mathrm{EM}}$	$<0.055 + 0.00045 \times E_{\mathrm{EM}}$ GeV
$E_{\mathrm{T}}^{\mathrm{cone}}/E_{\mathrm{T}}$	<0.1
Tight electron:	
As electron1 except	
$E/p(p_{\mathrm{T}} < 50\ \mathrm{GeV}/c)$	<2
L_{shr}	<0.2
χ^2_{strips}	<10
$Q \cdot \Delta x$	$> -3.0, <1.5$ cm
$\vert\Delta z\vert$	<3.0 cm
Plug electron:	
Track with silicon hits	
Not conversion	
$\vert\eta\vert$	$>1.2 < 2.0$
$E_{\mathrm{Had}}/E_{\mathrm{EM}}$	<0.055 GeV
$E_{\mathrm{T}}^{\mathrm{cone}}/E_{\mathrm{T}}$	<0.1
E/p	<3
PES 5/9 (see text)	>0.65
χ^2_{PEM}	<10

quality χ^2 normalized by the number of degrees of freedom in the track fitting. The efficiency of reconstructing a track is measured separately in calorimeter triggered $W \rightarrow e\nu$ events as described in [13].

TABLE III. Muon selection criteria.

Variable	Cut
Base muon:	
Central track	
E_{EM}	<2 GeV
$E_{\mathrm{Had}}(p_{\mathrm{T}} \geq 20\ \mathrm{GeV}/c)$	<6 GeV
$E_{\mathrm{Had}}(pT < 20\ \mathrm{GeV}/c)$	$<3.5 + pT/8$ GeV
Tight CMUP/CMX muon:	
Base muon	
$E_{\mathrm{T}}^{\mathrm{cone}}/p_{\mathrm{T}}$	<0.1
$\vert\Delta x_{CMU}\vert$ (CMUP)	<7 cm or $\chi^2 < 9$
$\vert\Delta x_{CMP}\vert$ (CMUP)	<5 cm or $\chi^2 < 9$
$\vert\Delta x_{CMX}\vert$ (CMX)	<6 cm or $\chi^2 < 9$
Loose CMUP/CMX muon:	
As muon1 except:	
$E_{\mathrm{T}}^{\mathrm{cone}}(p_{\mathrm{T}} < 20\ \mathrm{GeV}/c)$	<2 GeV
CMIO muon:	
Base muon	
Not fiducial to CMUP, CMX	
p_{T}	$\geq 10\ \mathrm{GeV}/c$
$E_{\mathrm{T}}^{\mathrm{cone}}/p_{\mathrm{T}}$	<0.1
$E_{\mathrm{EM}} + E_{\mathrm{Had}}$	>0.1 GeV

A candidate electron in the central region is a track pointing to an electromagnetic calorimeter cluster. If the ratio of the energy measured in the hadronic calorimeter to that measured in the electromagnetic calorimeter is small, we define it as a "loose" electron. Additional requirements on the shower shape and the energy to momentum ratio are imposed to select high purity, "tight" electrons. One such requirement, the lateral shower sharing profile (L_{shr}), compares the energy sharing between neighboring CEM towers to the expectation from test beam data. We also require the cluster to be close to the extrapolated track both in the r-ϕ plane ($Q \cdot \Delta x$, where Q is the lepton charge) and the r-z plane ($|\Delta z|$). In addition, we also restrict the χ^2 of the fit to the shower profile in the CES, and to test beam data. A similar procedure based on the χ^2 from comparing the tower energy distribution is applied to electrons reconstructed in the plug calorimeter. In this case only tracks within $|\eta| < 2$ and with silicon hits are accepted. The collimation of the shower shape in the PES is also restricted, by requiring that the energy in the middle five strips of a PES cluster should be more than 65% of the energy in all nine strips. If the track associated to the candidate electron is consistent with coming from a $\gamma \rightarrow e^+e^-$ conversion, the candidate electron is rejected. The photon conversion identification algorithm defines an electron as originating from a conversion if the azimuthal separation of the electron candidate and any oppositely charged track at the tangency point ($D_{xy} = R \times \Delta\phi$ where R is the conversion radius) is less than 0.2 cm and the difference in polar angle ($\Delta \cot\theta$) is smaller than 0.04. The measurement of the conversion identification efficiency is described in Sec. IV B 1.

Tracks with small energy deposits in the calorimeters and matched stubs [14] in the CMU and CMP (or CMX only) muon chambers are candidates for the CMUP (CMX) muon category. The matching between the extrapolated track and the stub in the chamber ($|\Delta x|$, where x is the local linear coordinate in the transverse plane) has to be within a certain range (refer to Table III). If a track has p_{T} less than 20 GeV$/c$, the effect of multiple scattering is enhanced and thus we set a less stringent requirement. For CMX muons we restrict our selection to tracks that pass through all eight super layers of the COT. The efficiency of finding a stub in the first place is measured separately and combined with the other identification measurements.

Other muons in an event are also included if they fall in the muon category called "central minimum ionizing objects" (CMIO's). This category is composed of tracks with p_{T} greater than 10 GeV$/c$ for which the track does not extrapolate to the fiducial region of the CMU and CMP or CMX chambers [15]. In this case we constrain the selection to muon candidate tracks with a nonzero calorimeter energy deposit to suppress tracks entering uninstrumented parts. This extends the muon coverage to $|\eta| < 1.5$, with lower efficiency and lower purity for $|\eta| > 1.2$.

Since leptons from $\tilde{\chi}_1^\pm$ and $\tilde{\chi}_2^0$ decays are expected to be well separated from each other and from other objects in the event, [16], we restrict our studies to isolated electrons and muons. To decide whether a lepton is isolated or not, we sum up the calorimeter transverse energy ($E_T^{\rm cone}$) in a cone of $\Delta R = \sqrt{\Delta\eta^2 + \Delta\phi^2} < 0.4$ around, but not including, the energy deposited by the lepton. We require $E_T^{\rm cone}$ to be less than 2 GeV for the loose CMUP and CMX muons. For other lepton categories, or if the muon p_T (electron E_T) is above 20 GeV/c (GeV), we require $E_T^{\rm cone}$ to be less than 10% of the muon p_T (electron E_T).

The primary data sample used to measure trigger and identification efficiencies for leptons with p_T $(E_T) >$ 20 GeV/c (GeV) is the single-electron or single-muon triggered sample with a p_T (E_T) threshold of 18 GeV/c (GeV) used for the analysis itself, as described in Sec. IV. Samples of simulated events needed in this study are also presented in Sec. IV. Additional data samples are used to measure efficiencies and misidentification probabilities for lower-energy leptons. These include samples collected with single-lepton trigger thresholds of 8 GeV/c for muon p_T and 8 GeV for electron E_T, and inclusive central jet samples collected with jet trigger thresholds at $E_T > 20$, 50, 70, and 100 GeV.

For high-p_T leptons, we measure the identification efficiencies using same-flavor, oppositely charged dilepton candidate events in the invariant mass window from 76 to 106 GeV/c^2. We require that at least one of those candidate leptons fulfills all the tight electron or tight CMUP/CMX criteria, defined in Tables II and III, respectively, and satisfying the trigger requirements. We then measure the efficiencies of our identification criteria on the other candidate lepton. In the case of $Z \to e^+e^-$ candidates we subtract background using same-charge dilepton events in the mass window. The effect of background subtraction is found to be negligible in the $Z \to \mu^+\mu^-$ sample [17].

The efficiency of low-p_T leptons is measured in Drell-Yan (DY) candidate events requiring same-flavor, oppositely charged leptons with $\Delta\phi(\ell_1\ell_2) > 160°$. In order to reject events in which a cosmic ray is reconstructed as a pair of muons, we require the timing of the track hits in the tracking system to be consistent with particles originating from the center of the detector and moving outwards, and reject events with significant $\not{E}_T$. At least one lepton candidate must pass all the identification criteria (to reduce instrumental and nonprompt background) and must satisfy the 8 GeV/c trigger requirements. We then measure the efficiency of the identification variables on the second lepton candidate in the event. In events in which both leptons pass the trigger requirements, we use both to determine the efficiency. The remaining background to be subtracted is estimated in events with lepton candidates of the same electric charge. As part of the cross checks and systematic uncertainties evaluation, we also verify the results using J/ψ and Υ candidate events and sideband subtraction, except for the isolation cut, as only the Drell-Yan selection gives well-isolated, prompt leptons with good statistics in the full p_T range. The resulting total identification efficiency ranges between 75% for forward electrons and 80% for central electrons to 90% for most muon categories.

In both observed events and Monte Carlo (MC) simulated events, we check for possible dependence of the efficiency of identifying leptons on additional factors: the number of primary vertices, the geometry of the detector, and changes in the detector performance and/or configuration over time. We include deviations as part of the uncertainty on lepton identification efficiency measurements. Figures 3 and 4 show examples of E_T (p_T) dependence in observed and simulated events. The dependence is mainly caused by photons radiated by the leptons; due to the p_T spectrum of Drell-Yan events, this effect is most visible in the 20–30 GeV range with our selection. The presence of extra photons means the isolation requirement (and for the muons, also the $E_{\rm EM}$ requirement) is not fully efficient in that p_T range for Drell-Yan events. This effect is adequately described by the Drell-Yan simulation. For very high-p_T electrons the efficiency measured in observed events is lower than the one measured in Drell-Yan simulated events due to the E/p cut becoming inefficient. For CMUP muons the efficiency measured in observed events and in simulated events shows the same dependency with respect to the muon transverse momentum. The efficiency measured in observed events is lower than the one measured in simulated ones because of mismodeling of multiple scattering. Discrepancies at the low-p_T end are caused

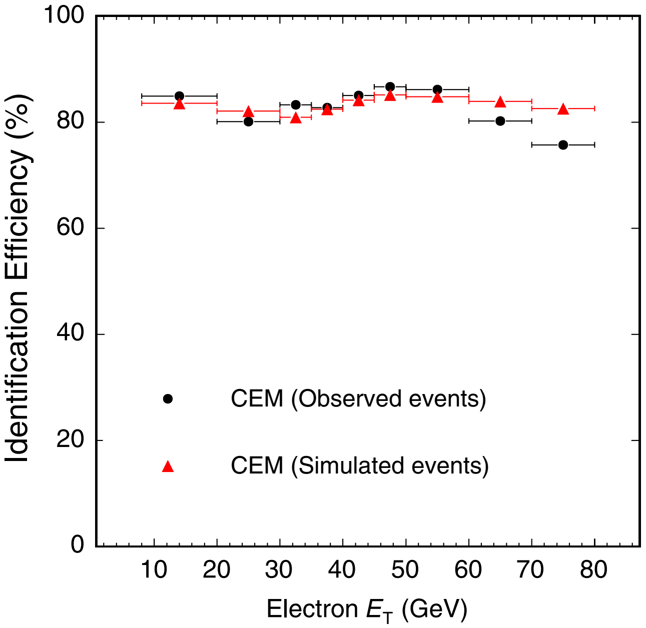

FIG. 3 (color online). The identification efficiency of tight electrons as a function of E_T using the Drell-Yan selection.

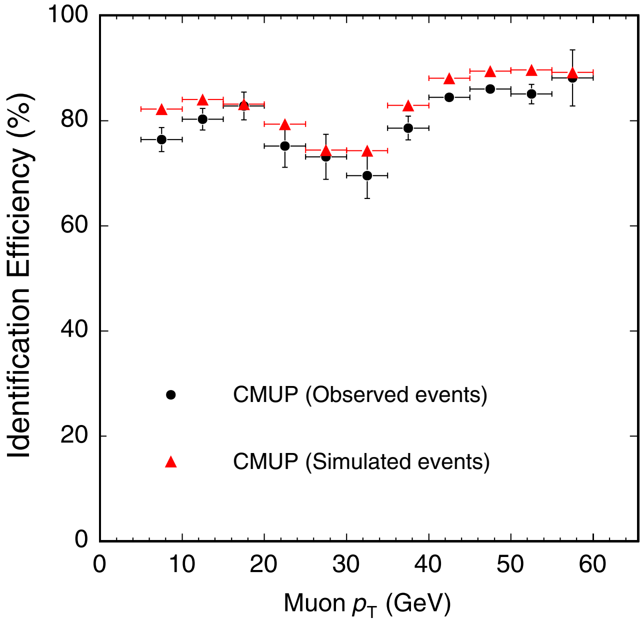

FIG. 4 (color online). The identification efficiency (including stub finding efficiency) of CMUP muons as a function of p_T using the Drell-Yan selection.

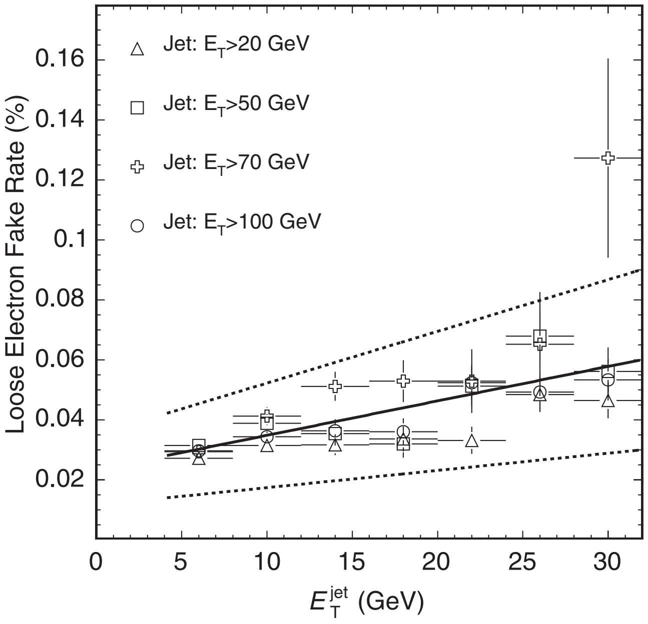

FIG. 5. Fake rate of loose central electrons. The solid line represents the linear fit to the average, and the dotted lines are ±50%.

by nonisolated, nonprompt background. Because the MC does not completely reproduce the identification efficiency found in the observed events, we define a scale factor (S_{ID}) as the ratio of the identification efficiency measured in the observed events to the identification efficiency found in the simulated samples. Typical scale factors applied to the MC predictions lie between 0.9 and 1.0 and are p_T and E_T dependent.

B. Probability of hadrons to be misidentified as leptons

A jet of hadrons is defined as a cluster of energy in the calorimeter and reconstructed using a fixed cone algorithm ($\Delta R = 0.4$). A jet can be misidentified as an electron if it consists of an energetic track pointing to a large energy deposit in the electromagnetic calorimeter. Charged kaons and pions with a late shower in the hadronic calorimeter, or those that decay in flight, can also mimic muons.

We use reconstructed jets to estimate the probability to misidentify them as electrons. In the study of misidentified muons, we use tracks with $E_T^{\rm cone} < 4$ GeV (called "isolated tracks"). The isolation is required to reduce the dependence on the sample composition. In the following we will refer to these jets and tracks as "fakeable objects." Since such fakeable objects originate from hadrons, we use the four data samples collected with jet-based triggers to measure their misidentification probability. We expect only a negligible contribution from inclusive W and Z production with the gauge bosons decaying into leptons, and do not apply any corrections. To avoid a trigger-induced bias, we remove the highest E_T jet from the collection of fakeable objects.

The misidentification probability, or fake rate, is calculated as the ratio of the number of identified lepton candidates over the number of fakeable objects. It is parametrized as a function of the transverse energy (transverse momentum) of the jet (isolated track) and averaged over the four jet data samples. The results for one of the electron and muon categories are shown in Figs. 5 and 6 respectively. The probability for misidentifying hadrons as muons is higher than that for electrons since the muon-type

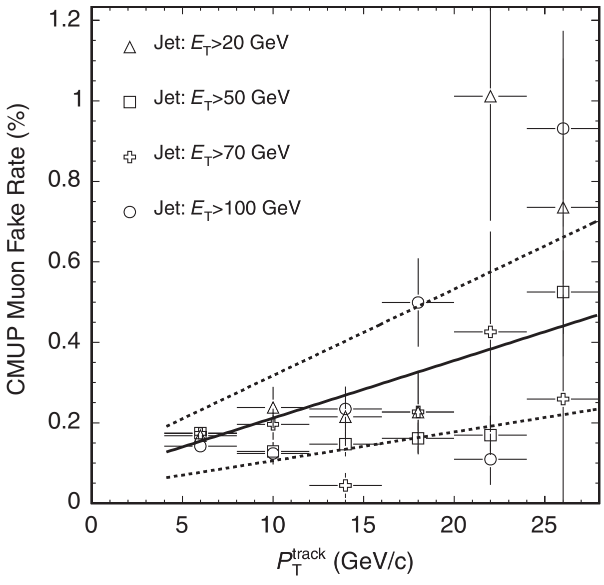

FIG. 6. Fake rate of CMUP muons. The solid line represents the linear fit to the average, and the dotted lines are ±50%.

fakeable object is based on an isolated track and thus more likely to pass our identification cuts. The application of these rates in the analysis is described in the next section. An uncertainty of 50% is assessed from the variation in the fake rates measured in the different jet data samples.

IV. SAMPLES OF OBSERVED AND SIMULATED EVENTS

A. Sample of observed events

The data used in this analysis were collected between March 2002 and February 2006 via electron-based and muon-based triggers. The former requires one central ($|\eta| < 1$) electron with $E_T > 18$ GeV, whereas the latter requires one $p_T > 18$ GeV/c central muon with a stub in both the CMU and CMP or in the CMX chambers. The data correspond to an integrated luminosity of 1.0 fb^{-1} and 0.7 fb^{-1} for the samples based on the electron and muon triggers, respectively.

B. Background samples

In the search based on three leptons and missing transverse energy, the SM backgrounds are $W\gamma$, WZ/γ^*, ZZ/γ^*, $t\bar{t}$, and Drell-Yan production, along with hadrons misidentified as leptons. The $b\bar{b}$ contamination is suppressed because the soft and typically nonisolated leptons from B decays are rejected by our lepton selection. The first set of backgrounds is estimated using a Monte Carlo technique, whereas the contribution from misidentified hadrons is measured using observed events (Sec. III). The simulated samples are generated using PYTHIA [18] version 6.216 with the underlying event model tuned to the CDF observed events [19]. In the case of the WZ sample, PYTHIA is used only for the parton showering and the hadronization of events that are generated with the leading-order matrix element program MADEVENT [20].

All simulated background samples were run through the full CDF detector simulation, which is based on the GEANT [21] framework, and the same reconstruction algorithm [22] that is used for the observed events. All simulation-driven background estimates are corrected for the different trigger efficiency (see, for instance, [13]) and identification efficiency measured in observed events with respect to the one in simulated events (Sec. III). An additional correction factor (S_{conv}) is needed for the Drell-Yan production, as explained in the next section.

To avoid overestimation of the background due to hadrons misidentified as leptons, we require each identified lepton in simulated events to originate from the hard interaction (this does not apply to the $t\bar{t}$ background where we only ask for three electrons or muons).

1. Drell-Yan production

Events from $Z/\gamma* \rightarrow \ell\ell$ constitute a background to our search if an additional lepton is present in the event. In this section we present the estimate of this background contribution when the third lepton comes from a photon radiated from one of the primary leptons, and has converted into an e^+e^- pair. In order to measure the efficiency of the conversion identification algorithm described in Sec. III, we collect a pure sample of candidate conversions using a calorimeter-based approach which does not rely on tracking information. The sample consists of identified electrons with p_T larger than 8 GeV/c (called "seed electrons") accompanied by an additional cluster found in the shower max detector. Since photons convert into oppositely charged electrons [23], we can predict the possible ϕ location of the cluster based on the charge of the seed electron. In Fig. 7 the "correct" and "incorrect" sides with respect to the seed electron are defined. Furthermore, the electrons from γ conversions are expected to have the same z coordinate at the CES, since the magnetic field B is along the z direction. Based on this, a candidate photon conversion is a seed electron accompanied by a CES cluster located on the correct side and having $|\Delta z_{\text{seed,cluster}}| < 20$ cm.

In order to improve the purity of the sample of candidate conversions, we reject events in which the seed electron comes from a W and is accompanied by a bremsstrahlung photon by requiring $\not{E}_T$ to be less than 10 GeV. Furthermore, if the invariant mass of the seed electron and a second same-flavor lepton in the event falls in the range from 50 to 106 GeV/c^2, the event is considered nonconversion background (Z + bremsstrahlung photon) and rejected. Events in which the bremsstrahlung photon converts are suppressed by rejecting electrons having the sum of the measured energy deposit in the electromagnetic calorimeter larger than the corresponding track momentum. Several other backgrounds mimic the conversion candidate signature, such as electrons accompanied by a π^0 (decaying into $\gamma\gamma$) or a $K^\pm$ (decaying in the detector and producing a shower in the electromagnetic calorimeter as well as in the hadronic calorimeter), or photons from extra interactions and jets. These components of the background are expected to contribute equally to the correct and

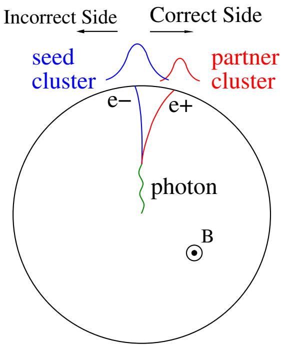

FIG. 7 (color online). Sketch of the r-ϕ view of a photon conversion signature with CES cluster locations. The magnetic field B is along the z direction.

incorrect sides. Consequently, they can be estimated by the number of events with clusters on the incorrect side. We measure the remaining background in the incorrect side through a fit and subtract it from the signal.

The results of the measurement performed on the observed and simulated events are shown in Fig. 8. The sources of inefficiency are mainly track reconstruction inefficiency in the region of low p_T, given the asymmetric nature of conversions, and rejections due to the thresholds on D_{xy} and $\Delta\cot\theta$. Several systematic uncertainties affect the measurement of the conversion identification efficiency, the most significant being the uncertainty on the normalization of the background and η dependence of the efficiency. The total uncertainty is 30% [24].

The conversion identification efficiency is lower in observed than in simulated events. To take this effect into account, we rescale the contribution of simulated events by S_{conv}, the ratio of the conversion identification inefficiency in observed events over the inefficiency in simulated events. We use the inefficiency rather than the efficiency since $S_{\text{conv}}(E_T)$ is applied to electrons originating from a nonidentified conversion in $Z/\gamma^* \to \ell\ell\gamma \to \ell\ell e^+e^-$. Only electrons for which the partner track p_T is larger than 0.7 GeV/c are corrected.

2. Background due to hadrons misidentified as leptons

In order to estimate the background contribution from events with two leptons and a misidentified lepton [25], we use the search data sample itself. We select dilepton events with at least one additional fakeable object separated from either identified leptons by $\Delta R > 0.4$. The number of observed events containing two identified leptons and one fakeable object is then scaled by the probability for the fakeable object to be misidentified as a lepton. We take into account the fact that there may be multiple fakeable objects per event.

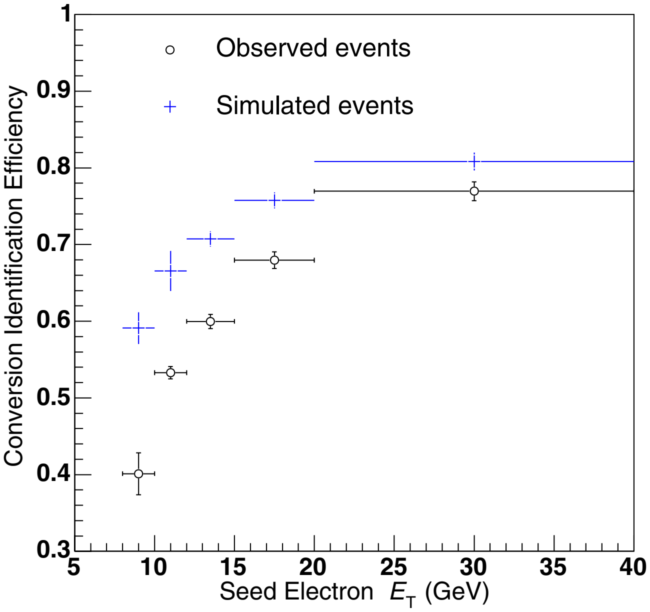

FIG. 8 (color online). Conversion identification efficiency as a function of the seed electron E_T.

C. SUSY samples generation

The chargino-neutralino cross section depends on the squark mass, as can be inferred from Fig. 1, whereas the branching ratio into three leptons and $\not{E}_T$ depends on the slepton masses. The chargino-neutralino scenario adopted to guide this trilepton analysis is taken from an mSUGRA model (referred to as the benchmark point). The benchmark point is characterized by $m_{1/2} = 180$ GeV/c^2, $m_0 = 100$ GeV/c^2, $A_0 = 0$, $\tan\beta = 5$, and $\mu > 0$. The parameters $m_{1/2}$ and m_0 indicate the unified gaugino and scalar masses, A_0 is the unified trilinear coupling of the theory, $\tan\beta$ is the ratio of the two Higgs vacuum expectation values, and μ is the Higgsino coupling. This benchmark point yields a typical mass spectrum above the LEP chargino mass limit, with charginos of 113 GeV/c^2, an LSP of 65 GeV/c^2, and the lightest stau ($\tilde{\tau}_1$) of 125 GeV/c^2. The next-to-leading order (NLO) production cross section calculated using PROSPINO 2.0 [26] is $\sigma = 0.64 \pm 0.06$ pb and the branching ratio into three leptons is 25%, as obtained from PYTHIA. The SUSY simulation sample is generated with PYTHIA version 6.216. In this mode, PYTHIA obtains the masses at the electroweak scale from the routine ISASUGRA (ISAJET [27] version 7.51).

While the benchmark point is used to study the event kinematics of chargino-neutralino associated production, three additional scenarios are used to fix squark and slepton masses and to interpret the results of our search. The modeling of the non-mSUGRA models is done by using SOFTSUSY 2.0.7 [28] as the input to PYTHIA 6.325, using the SUSY Les Houches Accord [29] framework. The SUSY contribution is corrected to take into account the different identification efficiency measured in observed and simulated events, the same way as for the backgrounds.

V. EVENT SELECTION

The samples of observed and simulated events are divided into four nonexclusive channels: $ee\ell$, $e\mu\ell$, $\mu\mu\ell$, and $\mu e\ell$, in which the first lepton listed is the one which passed the trigger requirements, and ℓ is an electron or muon. The lepton selection accepts also τ leptons, when they decay to electrons or muons.

In the $ee\ell$ and $e\mu\ell$ subsets, each event must contain at least one tight central electron with $E_T > 20$ GeV, consistent with the trigger object. The second lepton listed is either a loose electron or a plug electron with $E_T > 8$ GeV, or a muon with $p_T > 8$ GeV/c (10 GeV/c for CMIO's). In the $\mu\mu\ell$ and $\mu e\ell$ subsets [30], at least one lepton must be a CMUP or CMX muon with $p_T > 20$ GeV/c, and the second lepton can be either a loose central or plug electron with $E_T > 8$ GeV, or a muon with $p_T > 5$ GeV/c (10 GeV/c for CMIO's). The third lepton listed can be from any of the above categories with a common p_T (E_T) threshold of 5 GeV/c (5 GeV), except for CMIO's for which we always require $p_T > 10$ GeV/c.

A. Preselection

Based on the expected topology of chargino-neutralino events, we require all leptons to originate from the primary vertex, $|\Delta z(\ell_i, \text{primary vertex})| < 4$ cm and $|\Delta z(\ell_i, \ell_j)| < 4$ cm, and to be separate in η-ϕ space with $\Delta R > 0.4$.

The energy of candidate jets with $E_T > 5$ GeV and within $|\eta| < 2.5$ is corrected to take into account the geometry of the calorimeters and the nonlinearity of their response [31]. We do not include candidate jets that have a high electromagnetic to total energy ratio, consistent with being electrons. Each candidate jet is required to be far from all identified leptons in the event ($\Delta R > 0.4$). In the particular case of the $e\mu\ell$ channel, we reject events in which either the second or the third lepton is within 20 degrees of the jet axis.

The missing transverse energy, reconstructed from calorimeter towers with transverse energy larger than 0.1 GeV within $|\eta| < 3.6$, is corrected for muons because muons leave only small deposits of energy in the calorimeter. In the $\not{E}_T$ calculation, we take this effect into account by subtracting the transverse momenta of identified muon tracks from the $\not{E}_T$, after adding the average muon energy measured in the calorimeter and projected into the transverse plane. We suppress events with mismeasured $\not{E}_T$ by requiring the $\not{E}_T$ to be separated by at least 2 degrees in azimuth from the vectorial sum of the transverse momenta of the two highest p_T leptons, in events in which the second lepton is a muon. This selection is designed to reject potentially problematic Drell-Yan events where the lepton energies are mismeasured, producing missing transverse energy along the direction of the leptons. The underestimation or overestimation of the energy of a jet causes a spurious energy imbalance in the event, which affects the value of missing transverse energy. In order to remove such events, we require the smallest angle between $\not{E}_T$ and the axis of any candidate jet to be $\Delta\phi > 20$ degrees in the $\mu\mu\ell$ and $e\mu\ell$ channels.

In observed events with muons, cosmic rays are identified (and rejected) as two tracks aligned in the transverse plane satisfying quality and matching requirements. To reduce further the cosmic background in the $\mu\mu\ell$ and $\mu e\ell$ channels, we veto events in which the two highest p_T muons exhibit a three-dimensional angular separation larger than 178 degrees.

B. Kinematic selection

In order to achieve the best sensitivity, several event selection criteria are applied to reject the backgrounds.

An important discriminating variable is the invariant mass of same-flavor, oppositely charged leptons. The on-shell component of the Z production is suppressed by rejecting events with two leptons of the same flavor with a combined invariant mass in the window of 76 to 106 GeV/c^2. This selection also reduces the otherwise indistinguishable WZ background. Similarly, the low mass resonances such as J/ψ and Υ are removed by requiring a dilepton invariant mass larger than 15 GeV/c^2. The latter value is raised to 20GeV/c^2 for $ee\ell$ and $e\mu\ell$ events. Figure 9 shows the invariant mass of muon pairs in trilepton events.

In chargino-neutralino events in which the supersymmetric particles decay into leptons, we expect jet activity to come only from initial-state radiation (ISR). On the other hand, $t\bar{t}$ events always contain jets, a feature which distinguishes them from chargino-neutralino signal events. The $t\bar{t}$ background is reduced by rejecting events with more than one jet with $E_T > 20$ GeV.

Finally, SUSY events are characterized by significant missing transverse energy from the LSP's and the neutrinos. This pattern differs from Drell-Yan production of charged leptons, where only the $Z \to \tau\tau$ background exhibits real missing transverse energy. We require $\not{E}_T > 15$ GeV in order to remove the Drell-Yan events outside the Z mass window.

The resulting predictions of the signal yields in the benchmark point (S) and the accompanying SM backgrounds (B) after all cuts are given in Table IV. Typically the dominant background is due to real trilepton processes,

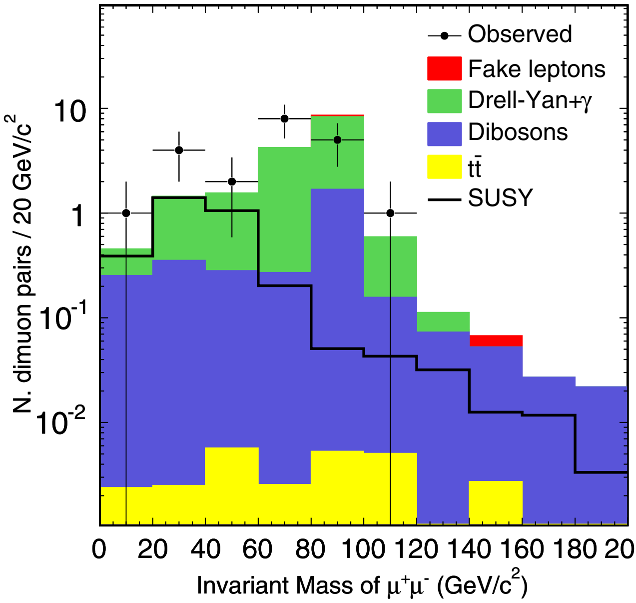

FIG. 9 (color online). Invariant mass of same-flavor, oppositely charged leptons in $\mu\mu\ell$ events. The SM backgrounds are stacked, while the benchmark SUSY signal is superimposed. Observed events are shown as points with error bars indicating the statistical uncertainty.

TABLE IV. Expected background and predicted signal for the mSUGRA benchmark point for all channels. The uncertainties shown are statistical only.

	$\mu\mu\ell$	$\mu e\ell$	$ee\ell$	$e\mu\ell$
Diboson	0.20 ± 0.02	0.44 ± 0.04	0.29 ± 0.02	0.17 ± 0.02
Drell-Yan $+\gamma$	0.22 ± 0.11	0.14 ± 0.06	0.14 ± 0.02	0.04 ± 0.04
Fake leptons	0.20 ± 0.02	0.17 ± 0.02	0.11 ± 0.01	0.05 ± 0.01
$t\bar{t}$	0.01 ± 0.01	0.02 ± 0.01	0.02 ± 0.01	0.02 ± 0.01
Total SM	0.64 ± 0.11	0.78 ± 0.08	0.56 ± 0.03	0.28 ± 0.05
Signal	1.60 ± 0.11	1.03 ± 0.06	1.22 ± 0.08	0.84 ± 0.07

while the $t\bar{t}$ contribution is negligible. The $\mu\mu\ell$ channel displays the highest sensitivity defined as $S/\sqrt{B}$. It can be inferred from the table that the prediction of Drell-Yan $+ \gamma$ is limited by the available number of simulated Drell-Yan events. This is due to a very high rejection factor for this background, and the resulting large uncertainty is taken into account later in the interpretation of the results.

VI. SYSTEMATIC UNCERTAINTIES

There are several systematic uncertainties which affect the numbers of predicted events and, consequently, the interpretation of the search result. The relative contributions vary from channel to channel and from signal to background. In the case of the background estimate, the largest uncertainty originates from the statistical uncertainty on the number of predicted events. These uncertainties are not negligible (up to 29%) due to the finite sample sizes and are included as independent sources of systematic uncertainty in the limit calculation described in Sec. IX. The uncertainty from the background due to misidentified leptons is determined from the precision of the fake rate measurement and it can be as large as 16%. For most lepton categories the systematic uncertainty due to the scale factors of the identification efficiency is a few percent, except for low-E_T plug electrons which have a 14% uncertainty. The jet energy scale [31] is varied within its uncertainty to estimate the impact on the jet multiplicity and on the correction of the missing transverse energy. The effect is between 2% and 7% depending on the channel. The integrated luminosity is measured with an accuracy of 6% [32] and it is used to normalize the contributions from simulated events. The ISR and final-state radiation (FSR) are modeled in the simulated samples and are subject to the uncertainty of the parton shower model. The effects of these uncertainties are determined from samples simulated with different ISR/FSR content [33], resulting in variations of up to 4% in selection acceptance. The cross sections and the event kinematics depend on the momenta of the incoming partons, whose spectra are parametrized by parton distribution functions (PDF's) obtained from a fit to the data from a number of experiments. We calculate the uncertainties on background rates by adding in quadrature the differences between each of the 40 CTEQ6 [34] systematic-variation eigenvectors and the nominal predictions. The effects on the cross sections and the acceptances are included. The resulting uncertainty on the background rates is 2%.

We also estimate the effect of the uncertainty in the theoretical cross-section predictions for diboson production (7%) [35] and $t\bar{t}$ production (10%) [36]. The individual contributions for background and SUSY signal are summarized in Table V, and the total systematic uncertainties for each channel are listed in Table VI.

TABLE V. Summary of systematic uncertainties.

	Resulting variation in	
Source	Signal	Background
Monte Carlo statistics	6%–10%	12%–29%
Hadron misidentification efficiency	···	9%–16%
Lepton identification efficiency	2%–7%	2%–14%
Jet energy scale	0.3%–3%	2%–7%
Luminosity	6%	4%–5%
ISR/FSR	2%–12%	3%–4%
PDF's	1%	2%–3%
Theoretical σ uncertainty	10%	4%–8%

TABLE VI. Combination of all systematic uncertainties in Table V for signal and background for each channel.

Systematic uncertainties	$\mu\mu\ell$	$\mu e\ell$	$ee\ell$	$e\mu\ell$
Background	28%	22%	20%	31%
Signal	13%	16%	14%	14%

VII. CONTROL SAMPLES

We test the SM predictions against the observed events by defining control samples in which we expect negligible contributions from SUSY events predicted by the benchmark point. We classify each event according to the missing transverse energy, the number of jets, the number of leptons, and, for ee and $\mu\mu$ events, the invariant mass of same-flavor, oppositely charged leptons. In particular, the subsample of events with two leptons is referred to as the "dilepton control region," and the subsample of events which contain three leptons is referred to as the "trilepton control region."

The normalization of the inclusive mass spectra for ee and $\mu\mu$ events, presented in Fig. 10 with the benchmark SUSY signal superimposed, demonstrates good understanding of the trigger and identification efficiencies along with the measurement of the integrated luminosity. The quality of the track and jet reconstruction can be assessed by comparing the missing transverse energy distributions in the observed and in the simulated events, as illustrated in Figs. 11 and 12. Same-flavor dilepton events are mainly DY $\mu^+\mu^-$ and DY e^+e^- as indicated by the softer $\not\!\!E_T$

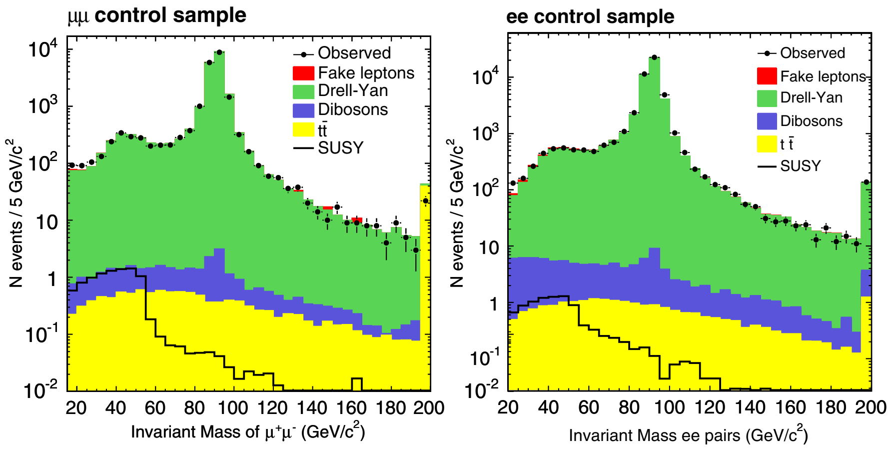

FIG. 10 (color online). Invariant mass of same-flavor lepton pairs. The SM backgrounds are stacked, while the benchmark SUSY signal is superimposed. Observed events are shown as points with error bars indicating the statistical uncertainty (overflows are added to the last bin).

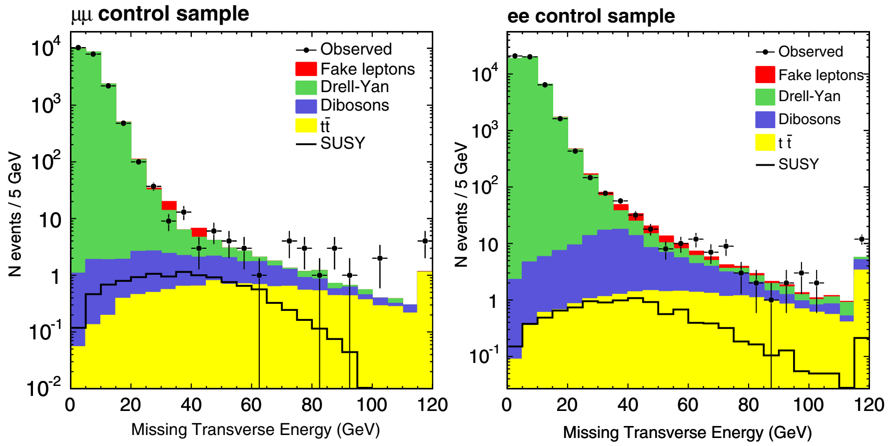

FIG. 11 (color online). Missing transverse energy in $\mu\mu$ and ee events. The SM backgrounds are stacked, while the benchmark SUSY signal is superimposed. Observed events are shown as points with error bars indicating the statistical uncertainty (overflows are added to the last bin).

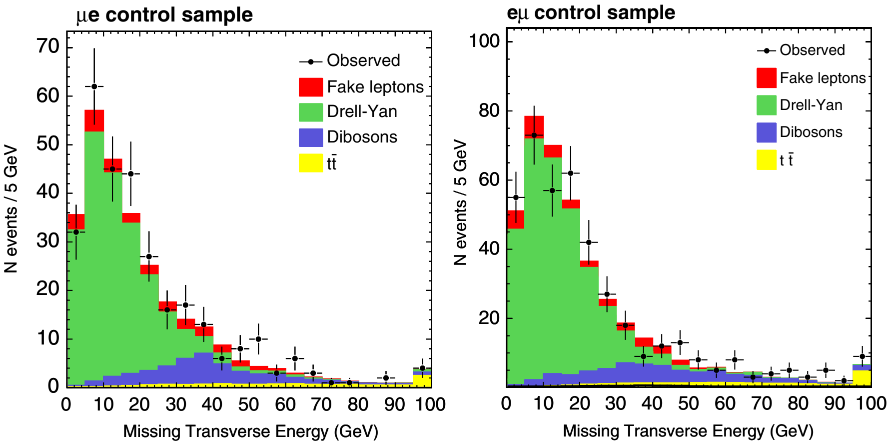

FIG. 12 (color online). Missing transverse energy in μe and $e\mu$ events. The SM backgrounds are stacked, while the benchmark SUSY signal is superimposed. Observed events are shown as points with error bars indicating the statistical uncertainty (overflows are added to the last bin). The expected benchmark SUSY signals in the μe and $e\mu$ channels are ~3 and ~6 events, respectively.

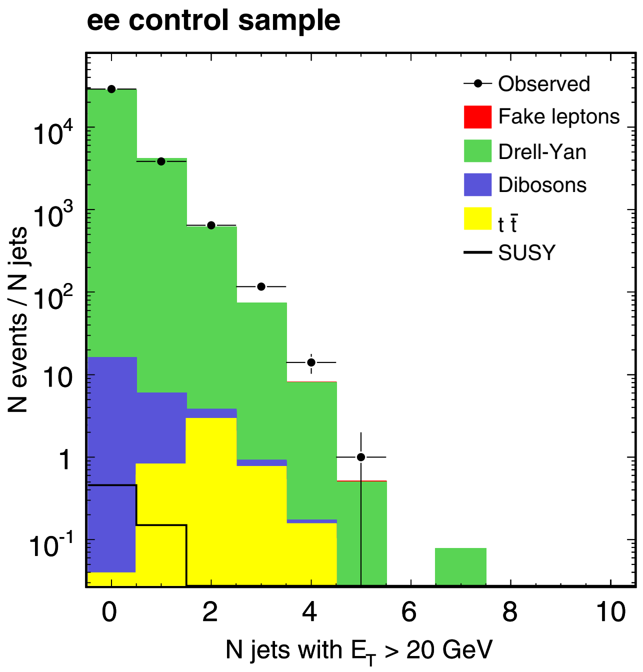

FIG. 13 (color online). Number of jets in ee events with invariant mass between 76 and 106 GeV$/c^2$. The SM backgrounds are stacked, while the benchmark SUSY signal is superimposed. Observed events are shown as points with error bars indicating the statistical uncertainty.

spectrum. In the μe and $e\mu$ channels, the broader $\not{E}_T$ spectrum originates from the leptonic decay of DY $\tau^+\tau^-$. Only for $\not{E}_T > 40$ GeV do other processes become important. The good agreement between the observed and simulated events shows that the $\not{E}_T$ resolution is simulated well. The jet multiplicity in DY e^+e^- candidate events is compared to the predictions based on initial-state radiation and extra interactions in Fig. 13. The event generator PYTHIA reproduces the observed data spectrum well in the region of our interest at low jet multiplicity, whereas for large jet multiplicity a NLO simulator with proper parton shower would be needed.

In Table VII we present examples of the numerical comparison between the observed events and the total expected background in 12 of the control samples we investigated:

(I) dielectron events with invariant mass outside the Z window and $\not{E}_T \leq 10$ GeV,
(II) dielectron events with invariant mass in the Z window and $\not{E}_T \geq 15$ GeV,
(III) dimuon events in the Z mass window and $\not{E}_T \leq 10$ GeV,
(IV) dimuon events in the Z mass window with at least two jets and $\not{E}_T \geq 15$ GeV,
(V) μe events with at least two jets and $\not{E}_T \geq 15$ GeV,
(VI) μe events with $\not{E}_T \geq 15$ GeV,
(VII) $e\mu$ events with $\not{E}_T \geq 15$ GeV and $\Delta\phi_{e,\mu} \leq 170°$,
(VIII) $e\mu$ events with $\not{E}_T \leq 10$ GeV,
(IX) $\mu\mu\ell$ events with $\not{E}_T \leq 10$ GeV,
(X) $\mu\mu\ell$ events in the Z mass window with $\not{E}_T \geq 15$ GeV,
(XI) $ee\ell$ events with $\not{E}_T \leq 10$ GeV,
(XII) $ee\ell$ events in the Z mass window with $\not{E}_T \geq 15$ GeV and at least two jets.

The trilepton control samples are particularly useful to verify the background from diboson production and misidentified hadrons. No significant discrepancies are seen between the predictions and the observations.

VIII. RESULTS

In Figs. 14 and 15 we illustrate the $\not{E}_T$ in trilepton events satisfying the invariant mass and jet requirements. After applying the final cut on $\not{E}_T$ we observe one event, and this is compatible with the SM predictions. The results, broken down by channels, are shown in Table VIII.

TABLE VII. Examples of control samples as listed in Sec. VII. The error on the number of events expected from SM backgrounds includes statistical and systematic uncertainties.

	Drell-Yan	Diboson, $t\bar{t}$	Misidentified hadrons	Total background	Observed
2 leptons:					
I	2359	1.9	33	2394 ± 314	2422
II	656	9.2	3.2	669 ± 159	638
III	15 587	1.5	<4.5	15 588 ± 2044	15 366
IV	29	2.0	<4.5	31 ± 4	31
V	1.6	9.1	1.0	11.7 ± 2.1	7
VI	76	49	12.5	138 ± 22	151
VII	22	16	1.2	38 ± 6	44
VIII	67	1.9	5.7	74 ± 9	62
3 leptons:					
IX	3.9	0.1	0.3	4.3 ± 1.3	4
X	0.5	1.1	0.5	2.1 ± 0.5	2
XI	3.3	0.2	0.4	3.9 ± 0.6	4
XII	0.01	0.01	0.04	0.06 ± 0.02	0

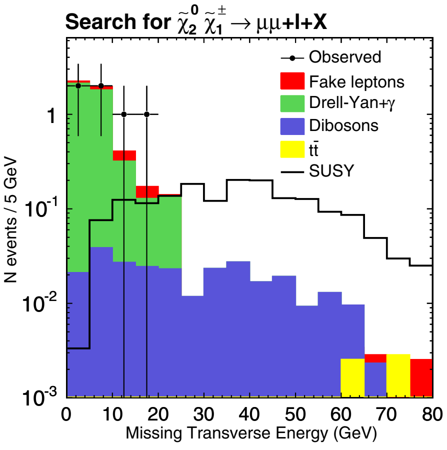

FIG. 14 (color online). Missing transverse energy before the final cut of 15 GeV in $\mu\mu\ell$ and $\mu e\ell$. The SM backgrounds are stacked, while the benchmark SUSY signal is superimposed. Observed events are shown as points with error bars indicating the statistical uncertainty.

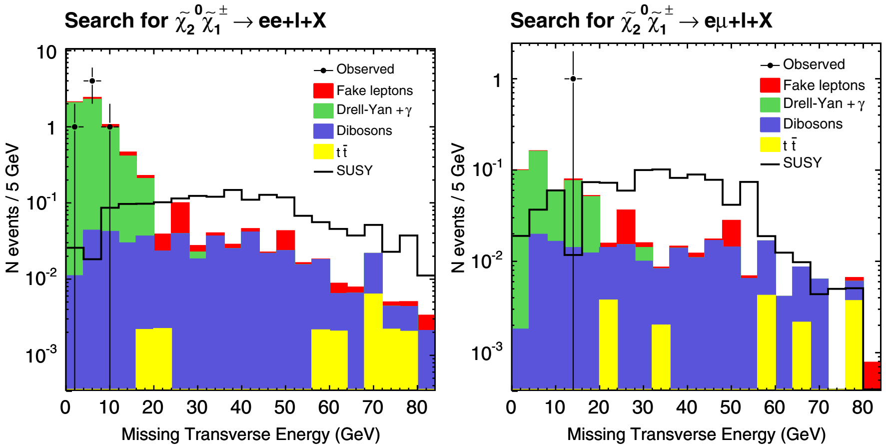

FIG. 15 (color online). Missing transverse energy before the final cut of 20 GeV in $ee\ell$ and $e\mu\ell$. The SM backgrounds are stacked, while the benchmark SUSY signal is superimposed. Observed events are shown as points with error bars indicating the statistical uncertainty.

In the candidate event we reconstruct three muons originating from the same primary vertex. The highest p_T muon is the CMX muon which fired the trigger. The second muon (oppositely charged, and at $\Delta\phi \sim 150$ degrees with respect to the leading muon) is a CMIO muon entering a nonfiducial part of the CMU and CMP muon chambers. The dimuon system has an invariant mass of 72 GeV$/c^2$. The third lepton selected is a CMUP muon. A jet was also produced in the hard interaction. The missing transverse energy is just above the threshold of our selection (15 GeV) with a value of 15.5 GeV. An additional 4 GeV electron candidate is reconstructed, but it comes from a different vertex. Figure 16 shows the r-ϕ view of the event in the CDF detector.

TABLE VIII. Summary of results for all channels. For a breakdown of individual background components, see Table IV.

	$\mu\mu\ell$	$\mu e\ell$	$ee\ell$	$e\mu\ell$
SM expectation	0.6 ± 0.2	0.8 ± 0.2	0.6 ± 0.1	0.3 ± 0.1
Observed	1	0	0	0

IX. INTERPRETATION

We combine the four channels to obtain limits on chargino-neutralino production cross sections and masses in three SUSY models. The calculation of the upper limit is based on the $\mathrm{CL_s}$ method [37,38] and incorporates the effect of the systematic uncertainties and correlations between channels, and between the signal and the background expectation for a given channel.

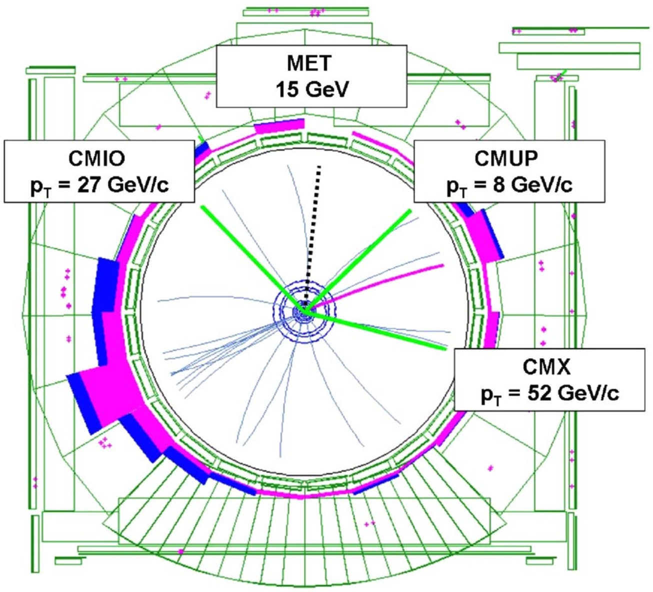

FIG. 16 (color online). The r-ϕ view of the $\mu\mu\mu$ candidate event in the CDF detector. Only tracks with $p_T \geq 1$ GeV$/c$ are shown in the central tracking detector. The three highlighted straight tracks are labeled with the muon category and momentum. The dotted black line shows the direction of the $\not{E}_T$ (MET). The energy deposit is illustrated in the histograms around the tracking view. Innermost (light) towers show the electromagnetic energy in the calorimeter towers; outermost (dark) show the hadronic component of the energy.

In the combination process, each simulated event and each observed event are interpreted in at most one channel. The overlap in the channels described above is removed by assigning SUSY simulated events selected by several analyses to the analysis with the highest sensitivity. For a given channel the acceptance is defined as the ratio of the number of events in the SUSY simulated sample satisfying the analysis requirements over the number of events where chargino $\tilde{\chi}_1^{\pm}$ and neutralino $\tilde{\chi}_2^0$ decay leptonically ($\tilde{\chi}_1^{\pm} \rightarrow \ell\nu\tilde{\chi}_1^0$, and $\tilde{\chi}_2^0 \rightarrow \ell\ell\tilde{\chi}_1^0$, with $\ell = e, \mu, \tau$). In the acceptance calculation the overlap is taken into account. The exclusive background is obtained by rescaling the inclusive background by $\frac{A^{\rm excl}_{\rm SUSY}}{A^{\rm incl}_{\rm SUSY}}$, where $A^{\rm excl}_{\rm SUSY}$ ($A^{\rm incl}_{\rm SUSY}$) is the exclusive (inclusive) acceptance for the SUSY signal. This procedure is adopted to simplify the combination with several other channels while ensuring no double counting. We have checked that this is equivalent to the background estimate obtained by excluding shared events within 3%. No observed events are shared.

We first explore the upper limit on the signal cross section times branching ratio in an mSUGRA scenario defined by the following parameters: $m_0 = 60$ GeV$/c^2$, $A_0 = 0$, $\tan\beta = 3$, $\mu > 0$, and $m_{1/2}$ varying between 162 and 230 GeV$/c^2$. These parameters were chosen to maximize chargino-neutralino trilepton production, $\sigma(\tilde{\chi}_1^{\pm}\tilde{\chi}_2^0) \times \mathrm{BR}(\tilde{\chi}_1^{\pm}\tilde{\chi}_2^0 \rightarrow \ell\nu\tilde{\chi}_1^0\ell\ell\tilde{\chi}_1^0)$. In this scenario the two-body decays of the charginos and neutralinos into sleptons are kinematically allowed.

The second model we investigate is a generic minimal supersymmetric standard model (MSSM) fully defined at the electroweak scale (MSSM-W/Z). Chargino and neutralino decays through virtual W and Z bosons dominate, resulting in three-body decays and branching ratios similar to those of standard model W's and Z's [39]. In this case only the production cross section, but not the leptonic branching ratio, is dependent on the gaugino masses.

As done in previous analyses [7], we also investigate a scenario in which there is no slepton mixing and the selectron, smuon, and stau have a degenerate mass ranging from 101 to 118 GeV$/c^2$ as $m_{1/2}$ varies between 162 and 230 GeV$/c^2$ (MSSM-no-mix). The important difference in branching ratios between mSUGRA and MSSM-no-mix scenarios is illustrated in Fig. 17. In addition to changing the mixing parameter, we also increased the mSUGRA

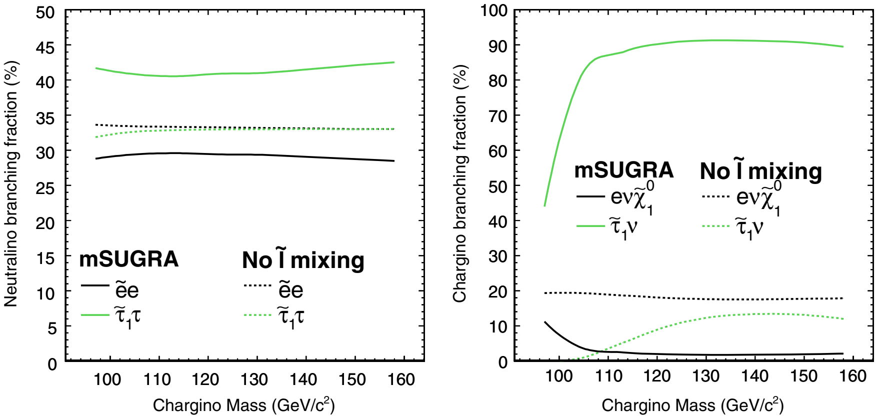

FIG. 17 (color online). Branching ratios for neutralino $\tilde{\chi}_2^0$ (top panel) and chargino $\tilde{\chi}_1^+$ (bottom panel) in the mSUGRA and MSSM-no-mix scenarios for different slepton flavors. The $\tilde{\chi}_1^+$ has $\mathrm{BR}(\ell\nu\tilde{\chi}_1^0) \approx \mathrm{BR}(\bar{d}u\tilde{\chi}_1^0) = \mathrm{BR}(\bar{s}c\tilde{\chi}_1^0)$ in both scenarios.

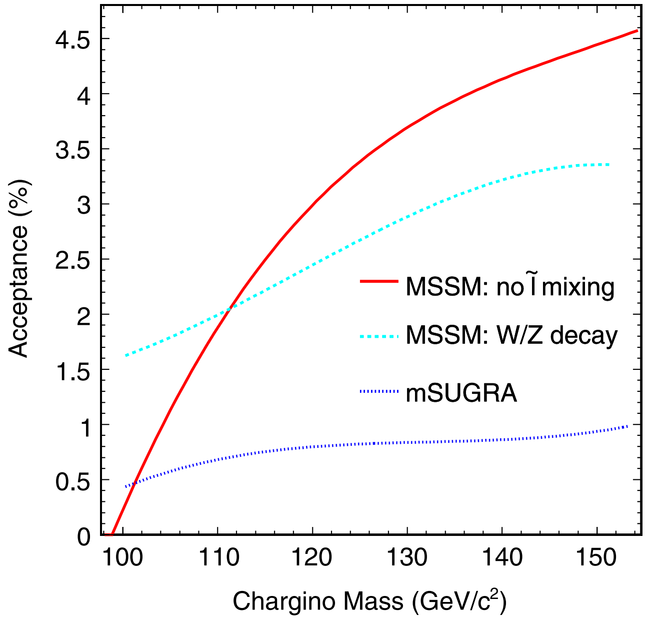

FIG. 18 (color online). Total acceptance of the channels for the three scenarios considered.

parameter m_0 to 70 GeV/c^2, to delay the turn-on of the $\tilde{\chi}_1^{\pm} \rightarrow \tilde{\nu}\ell$ decay modes as the chargino mass increases.

The total acceptance of the channels described in this paper for the three scenarios is shown in Fig. 18 as a function of the chargino mass. In the MSSM-W/Z scenario the acceptance is higher than the acceptance in the mSUGRA scenario but the mass dependence is similar. Our sensitivity to the MSSM-W/Z is low due to the overall reduced leptonic branching ratio. The acceptance in the mSUGRA scenario is suppressed because of the high branching ratio into staus: the $\tilde{\tau}_1$ mass, which varies between 92 and 110 GeV/c^2 as $m_{1/2}$ increases from 162 to 230 GeV/c^2, is smaller than the first and second generation slepton masses because of the mixing among the third-generation sleptons. The MSSM-no-mix is a more optimistic scenario for our selection, as it increases the number of electrons and muons in the final state.

The observed and expected limits on the cross sections times branching ratios are calculated at the 95% confidence level, and the mass limits in the different scenarios are obtained by including the theory cross-section uncertainty in the expected and observed limit calculations, and taking the intersection between those and the central theory curve. The 95% C.L. limits for the mSUGRA scenario and MSSM-W/Z scenario are presented in Figs. 19 and 20. The analyses are not sensitive to chargino and neutralino production in these models. For the MSSM-no-mix scenario we extend the current chargino mass limit up to 151 GeV/c^2 at 95% C.L., consistent with the expected sensitivity of 148 GeV/c^2 (Fig. 21). Our analysis is not sensitive to chargino masses below ~110 GeV/c^2. This mass range represents a transition to a region of the SUSY

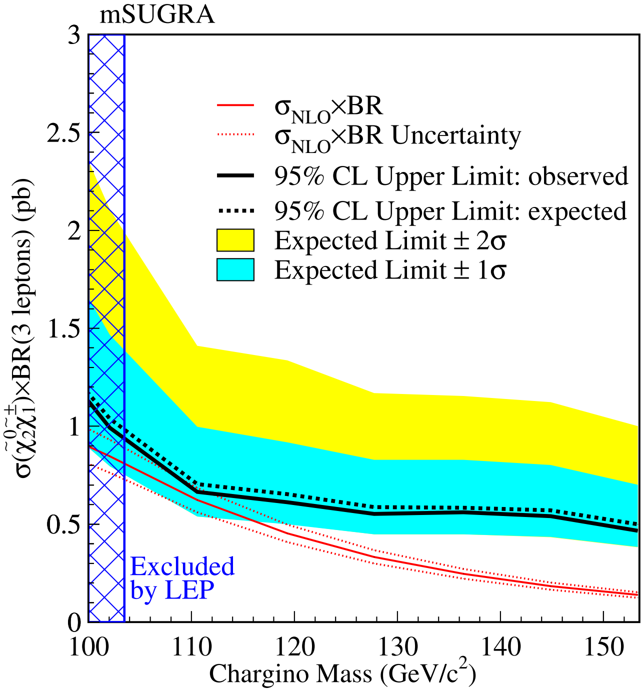

FIG. 19 (color online). Exclusion limits for the mSUGRA scenario. The bands indicate the range of expected limits given the possible outcomes that could have been observed if a signal were not there.

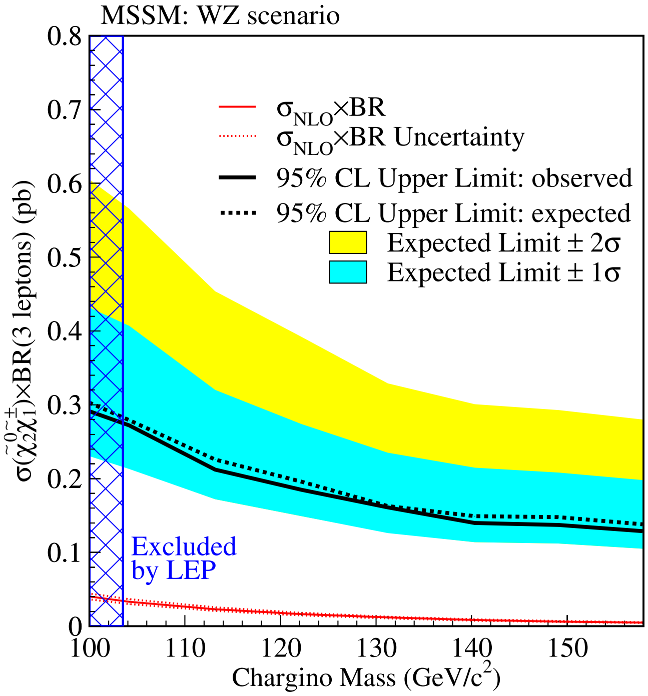

FIG. 20 (color online). Exclusion limits for the MSSM-W/Z scenario. The bands indicate the range of expected limits given the possible outcomes that could have been observed if a signal were not there.

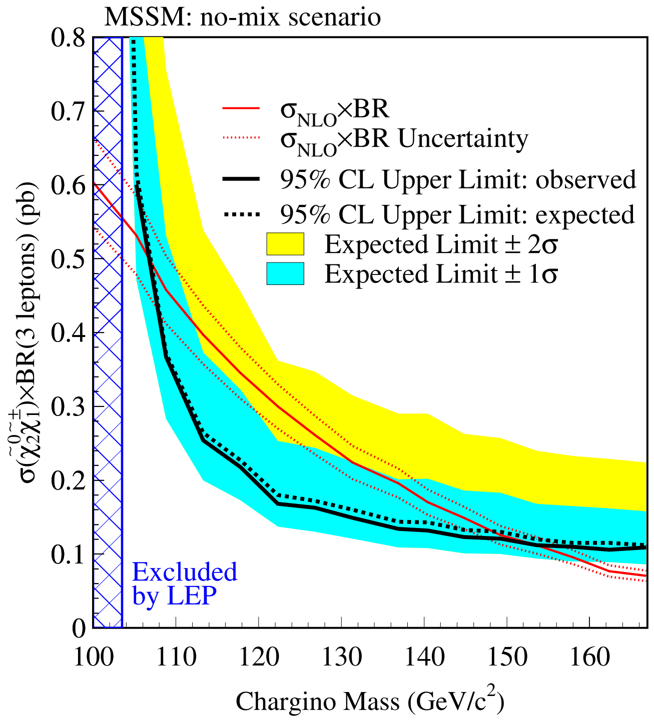

FIG. 21 (color online). Exclusion limits for the MSSM-no-mix scenario. The bands indicate the range of expected limits given the possible outcomes that could have been observed if a signal were not there.

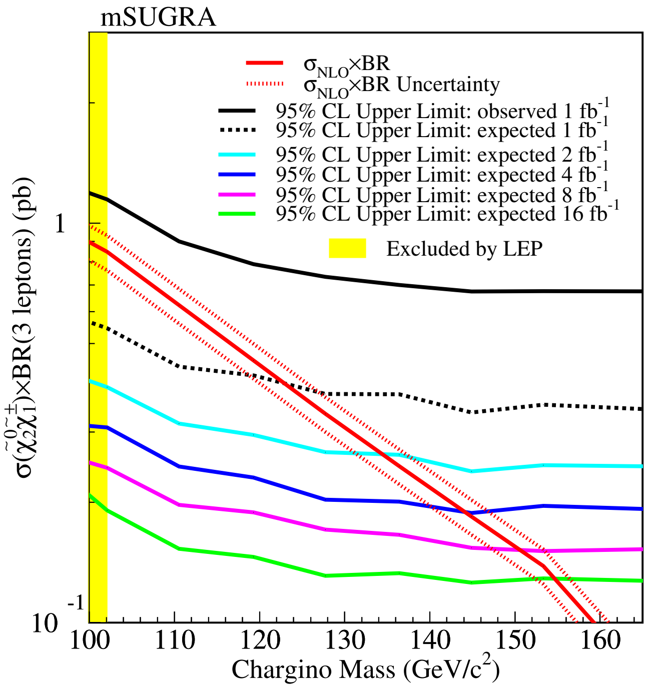

FIG. 22 (color online). Projection of the current expected result with increased data size for the mSUGRA scenario assuming no signal is observed. Also shown is the current observed limit (top solid line).

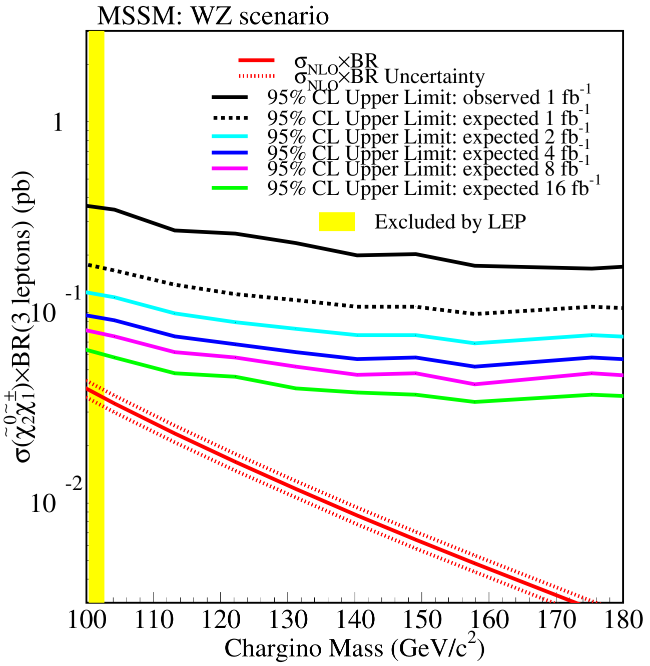

FIG. 23 (color online). Projection of the current expected result with increased data size for the MSSM-W/Z scenario assuming no signal is observed. Also shown is the current observed limit (top solid line).

parameter space with three-body decays of $\tilde{\chi}_2^0$, giving rise to very low p_T leptons (on average, below 2 GeV$/c$).

Projections for the CDF combined trilepton analysis

The analyses presented in this paper have been combined with other CDF searches sensitive to associated chargino-neutralino production as reported in [10,40]. The observed limits for the combination are less stringent than the one calculated for the high-p_T analysis due to slight excesses in the other channels.

To assess the future reach at CDF, we also extrapolate the sensitivity of the combined analysis assuming larger data sets. Figures 22–24 are the projected expected limits in the three models with 2, 4, 8, and 16 fb^{-1} of data collected, but assuming unchanged analyses. In the plots we also assume that the systematic uncertainties will scale inversely with the luminosity. Using 4 fb^{-1} of data, the CDF experiment has the potential to exclude chargino masses below 140 GeV$/c2$ and 180 GeV$/c2$ in the mSUGRA and MSSM-no-mix scenarios, respectively.

X. SUMMARY

We searched for the associated production of charginos and neutralinos in final states with one high-p_T electron or muon, and two additional leptons. The observed data

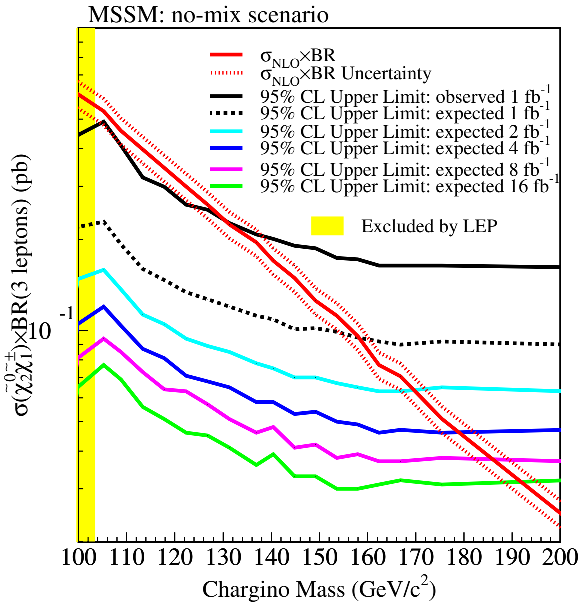

FIG. 24 (color online). Projection of the current expected result with increased data size for the MSSM-no-mix scenario assuming no signal is observed. Also shown is the current observed limit (top solid line).

counts are consistent with the expectations from the standard model backgrounds, and we set limits on the production cross section times branching ratio. In the MSSM model with no slepton mixing and degenerate slepton masses, $m_0 = 70\ \mathrm{GeV}/c^2$, $\tan\beta = 3$, and $\mu > 0$, we set a 95% C.L. limit on the chargino mass at 151 GeV/c^2.

ACKNOWLEDGMENTS

We thank the Fermilab staff and the technical staffs of the participating institutions for their vital contributions. This work was supported by the U.S. Department of Energy and National Science Foundation; the Italian Istituto Nazionale di Fisica Nucleare; the Ministry of Education, Culture, Sports, Science and Technology of Japan; the Natural Sciences and Engineering Research Council of Canada; the National Science Council of the Republic of China; the Swiss National Science Foundation; the A. P. Sloan Foundation; the Bundesministerium für Bildung und Forschung, Germany; the Korean Science and Engineering Foundation and the Korean Research Foundation; the Science and Technology Facilities Council and the Royal Society, United Kingdom; the Institut National de Physique Nucleaire et Physique des Particules/CNRS; the Russian Foundation for Basic Research; the Comisión Interministerial de Ciencia y Tecnología, Spain; the European Community's Human Potential Programme; the Slovak R&D Agency; and the Academy of Finland.

---

[1] J. Wess and B. Zumino, Phys. Lett. **49B**, 52 (1974).
[2] For a review, see S. P. Martin, arXiv:hep-ph/9709356.
[3] D. Z. Freedman *et al.*, Phys. Rev. D **13**, 3214 (1976).
[4] R parity is defined as $R_P = (-1)^{3(B-L)+2s}$, where B is the baryon number, L is the lepton number, and s is the spin. A SM particle therefore carries $R_P = +1$ and its SUSY partner $R_P = -1$.
[5] LEP Supersymmetry Working Group, ALEPH, DELPHI, L3, and OPAL experiments, Report No. LEPSUSYWG/01-03.1 (http://lepsusy.web.cern.ch/lepsusy/Welcome.html).
[6] LEP Supersymmetry Working Group, ALEPH, DELPHI, L3, and OPAL experiments, Report No. LEPSUSYWG/02-06.2 (http://lepsusy.web.cern.ch/lepsusy/Welcome.html).
[7] V. Abazov *et al.* (D0 Collaboration), Phys. Rev. Lett. **95**, 151805 (2005).
[8] M. Carena *et al.*, Rev. Mod. Phys. **71**, 937 (1999).
[9] Missing transverse energy, $\not{E}_T$, is defined as the magnitude of $-\sum_i E_T^i \hat{n}_i$, where $\hat{n}_i$ is the unit vector in the azimuthal plane that points from the interaction point to the ith calorimeter tower, and E_T^i the transverse energy in that tower.
[10] T. Aaltonen *et al.* (CDF Collaboration), Phys. Rev. Lett. **99**, 191806 (2007).
[11] D. Acosta *et al.* (CDF Collaboration), Phys. Rev. D **71**, 032001 (2005).
[12] P. Lukens *et al.* (CDF Collaboration), Report No. FERMILAB-TM-2198, 2003.
[13] A. Abulencia *et al.* (CDF Collaboration), J. Phys. G **34**, 2457 (2007).
[14] A pattern of hits in a muon chamber passing certain quality criteria is defined as a "stub."
[15] This includes cases where there is a stub in the BMU, CMU, or CMP chambers only.
[16] V. Barger *et al.*, arXiv:hep-ph/0003154v1.
[17] A. Abulencia *et al.* (CDF Collaboration), Phys. Rev. D **74**, 072006 (2006).
[18] T. Sjöstrand *et al.*, J. High Energy Phys. 05 (2006) 026.
[19] M. Dobbs *et al.*, The QCD/SM Working Group Summary Report, arXiv:hep-ph/0403100.
[20] F. Maltoni and T. Stelzer, J. High Energy Phys. 02 (2003) 027.
[21] R. Brun *et al.*, GEANT: Simulation Program for Particle Physics Experiments. User Guide and Reference Manual, Report No. CERN-DD-78-2-REV.
[22] E. Gerchtein and M. Paulini, Report No. CHEP-2003-TUMT005, 2003.
[23] We refer to both electrons and positrons as electrons.
[24] A. Abulencia *et al.* (CDF Collaboration), Phys. Rev. Lett. **98**, 131804 (2007).
[25] Given the small misidentification probability per fakeable

object ($\mathcal{P} \sim 10^{-3}$), it is unlikely to find two misidentified leptons in the same event ($\mathcal{P} \sim 10^{-6}$).

[26] W. Beenakker *et al.*, Phys. Rev. Lett. **83**, 3780 (1999).

[27] H. Baer *et al.*, ISAJET manual, arXiv:hep-ph/0001086.

[28] B. C. Allanach, Comput. Phys. Commun. **143**, 305 (2002).

[29] P. Z. Skands *et al.*, J. High Energy Phys. 07 (2004) 036.

[30] A. Canepa, Ph.D thesis, Purdue University [Report No. FERMILAB-THESIS-2006-49, 2006 (unpublished)].

[31] A. Bhatti *et al.*, Nucl. Instrum. Methods Phys. Res., Sect. A **566**, 375 (2006).

[32] S. Klimenko, J. Konigsberg, and T. Liss, Report No. FERMILAB-FN-0741, 2003; D. Acosta *et al.*, Nucl. Instrum. Methods Phys. Res., Sect. A **494**, 57 (2002).

[33] A. Abulencia *et al.* (CDF Collaboration), Phys. Rev. D **73**, 112006 (2006).

[34] H. L. Lai *et al.*, Eur. Phys. J. C **12**, 375 (2000).

[35] J. M. Campbell and R. K. Ellis, Phys. Rev. D **60**, 113006 (1999).

[36] R. Bonciani *et al.*, Nucl. Phys. **B529**, 424 (1998).

[37] T. Junk, Nucl. Instrum. Methods Phys. Res., Sect. A **434**, 435 (1999).

[38] A. L. Read, J. Phys. G **28**, 2693 (2002).

[39] For instance, we set $\mathrm{BR}(\tilde{\chi}_1^+ \to \ell\nu\tilde{\chi}_1^0) = \mathrm{BR}(W \to \ell\nu)$ and $\mathrm{BR}(\tilde{\chi}_2^0 \to \ell\ell\tilde{\chi}_1^0) = \mathrm{BR}(Z \to \ell\ell)$.

[40] A. Abulencia *et al.* (CDF Collaboration), Phys. Rev. Lett. **98**, 221803 (2007).